

Kinetic Mixing, Dark Photons and Extra Dimensions III: Brane Localized Dark Matter

Thomas G. Rizzo and George N. Wojcik [†]

SLAC National Accelerator Laboratory
2575 Sand Hill Rd., Menlo Park, CA, 94025 USA

Abstract

Extra dimensions have proven to be a very useful tool in constructing new physics models. In earlier work, we began investigating toy models for the 5-D analog of the kinetic mixing/vector portal scenario where the interactions of dark matter, taken to be, *e.g.*, a complex scalar, with the brane-localized fields of the Standard Model (SM) are mediated by a massive $U(1)_D$ dark photon living in the bulk. These models were shown to have many novel features differentiating them from their 4-D analogs and which, in several cases, avoided some well-known 4-D model building constraints. However, these gains were obtained at the cost of the introduction of a fair amount of model complexity, *e.g.*, dark matter Kaluza-Klein excitations. In the present paper, we consider an alternative setup wherein the dark matter and the dark Higgs, responsible for $U(1)_D$ breaking, are both localized to the ‘dark’ brane at the opposite end of the 5-D interval from where the SM fields are located with only the dark photon now being a 5-D field. The phenomenology of such a setup is explored for both flat and warped extra dimensions and compared to the previous more complex models.

arXiv:2006.06858v1 [hep-ph] 11 Jun 2020

[†]rizzo, gwojci03@slac.stanford.edu

1 Introduction

The nature of dark matter (DM) and its possible interactions with the fields of the Standard Model (SM) is an ever-growing mystery. Historically, Weakly Interacting Massive Particles (WIMPs) [1], which are thermal relics in the \sim few GeV to \sim 100 TeV mass range with roughly weak strength couplings to the SM, and axions [2, 3] were considered to be the leading candidates for DM as they naturally appeared in scenarios of physics beyond the Standard Model (BSM) that were constructed to address other issues. Important searches for these new states are continuing to probe ever deeper into the remaining allowed parameter spaces of these respective frameworks. However, the null results so far have prompted a vast expansion in the set of possible scenarios [4, 5] which span a huge range in both DM masses and couplings. In almost all of this model space, new forces and, hence, new force carriers must also exist to mediate the interactions of the DM with the SM which are necessary to achieve the observed relic density [6]. One way to classify such interactions is via “portals” [7] of various mass dimension that result from integrating out some set of heavy fields; at the renormalizable level, the set of such portals is known to be quite restricted [7, 8]. In this paper, we will be concerned with the implications of the vector boson/kinetic mixing (KM) portal, which is perhaps most relevant for thermal DM with a mass in the range of a \sim few MeV to \sim few GeV and which has gotten much attention in the recent literature [8]. In the simplest of such models, a force carrier, the dark photon (DP), the gauge field corresponding to a new gauge group, $U(1)_D$, under which SM fields are neutral, mediates the relevant DM-SM interaction. This very weak interaction is the result of the small KM between this $U(1)_D$ and the SM hypercharge group, $U(1)_Y$, which is generated at the one-(or two)-loop level by a set of BSM fields, called portal matter (PM) [8, 9], which carry charges under both gauge groups. In the IR, the phenomenology of such models is well-described by suitably chosen combinations of only a few parameters: the DM and DP masses, $m_{DM,V}$, respectively, the $U(1)_D$ gauge coupling, g_D and ϵ , the small dimensionless parameter describing the strength of the KM, $\sim 10^{-(3-4)}$. Frequently, and in what follows below, this scenario is augmented to also include the dark Higgs (DH) boson, whose vacuum expectation value (vev) breaks $U(1)_D$ thus generating the DP mass. This introduces two additional parameters with phenomenological import: the DH mass itself and the necessarily (very) small mixing between the DH and the familiar Higgs of the SM. Successfully extending this scenario to a completion in the UV while avoiding any potential issues that can be encountered in the IR remains an interesting model-building problem.

Extra dimensions (ED) have proven themselves to be a very useful tool for building interesting models of new physics that can address outstanding issues that arise in 4-D [10]. In a previous pair of papers [11, 12], hereafter referred to as I and II respectively, we considered the implications of extending this familiar 4-D KM picture into a (flat) 5-D scenario where it was assumed that the DM was either a complex scalar, a Dirac fermion or a pseudo-Dirac fermion with an $O(1)$ mass splitting. In all cases we found some unique features of the 5-D setup, *e.g.*, the existence of strong destructive interference between the exchanges of Kaluza-Klein (KK) excitations of the DP allowing for light Dirac DM, which is excluded by CMB [13, 14] constraints in 4-D, new couplings of the split pseudo-Dirac states to the DP that avoids co-annihilation suppression found in 4-D [15], or the freedom to choose appropriate 5-D wave function boundary conditions, *etc.*, all of which helped us to avoid some of the model building constraints from which the corresponding 4-D KM scenario can potentially suffer.

The general structure of the model setups considered previously in I and II followed from some rather basic assumptions: (i) The 5-D space is a finite interval, $0 \leq y \leq \pi R$, that is bounded by two branes, upon one of which the SM fields reside while the DP lives in the full 5-D bulk. This clearly implies that the $U(1)_D - U(1)_Y$ KM must solely occur on the SM brane. The (generalization of) the usual field redefinitions required to remove this KM in order to obtain canonically normalized fields then naturally leads to the existence of a very small, but *negative* brane localized kinetic term (BLKT) [16] for the DP which itself then leads to a tachyon and/or ghost field in its Kaluza-Klein (KK) expansion. We are then led to the necessary conclusion that an $O(1)$ *positive* BLKT must already exist to remove this problem; the necessity of such a term was then later shown to be also very useful for other model building purposes. (ii) A simple way to avoid any significant mixing between SM Higgs, H , and the dark Higgs, S which is employed in 4-D to generate the DP mass, is to eliminate the need for the dark Higgs to exist. This then removes the necessity of fine-tuning the parameter λ_{HS} in the scalar potential describing the $\sim S^\dagger S H^\dagger H$

interaction in order to avoid a large branching fraction for the invisible width for the SM Higgs, H [17,18]. As is well known, one can employ appropriate (mixed) boundary conditions (BC) on the 5-D DP wave function on both branes to break the $U(1)_D$ symmetry and generate a mass for the lowest lying DP KK mode [19] without the presence of the dark Higgs. These BC generically have the form (in the absence of BLKTs or other dynamics on either brane) $v(y)|_1 = 0$, $\partial v(y)|_2 = 0$ where v is the 5-D DP wavefunction, y describing the co-ordinate in the new extra dimension as above and $|_i$ implies the evaluation of the relevant quantity on the appropriate brane. Since the SM exists and the corresponding KM happens on one of these branes, it is obvious the v cannot vanish there, so we identify the location of the SM with brane 2. It is then also obvious that the DM itself cannot live on brane 1 otherwise it would no longer interact with either the DP or, through it, with the SM, so the DM must *also* reside in the bulk, have its own set of KK excitations and, for phenomenological reasons, its own, somewhat larger BLKT along with constrained boundary conditions. While allowing us to successfully circumvent some of the possible problems associated with analogous 4-D setup, this arrangement leads to a rather unwieldy structure. Can we do as well (or better) with a less cumbersome setup? This is the issue we address in the current paper.

The complexity of the previously described structure follows directly from (ii), *i.e.*, employing boundary conditions to break $U(1)_D$ so that there is no dark Higgs-SM Higgs mixing (as there is no dark Higgs with which to mix). In the present analysis, we consider an alternative possibility which also naturally avoids this mixing in an obvious way, *i.e.*, localizing the dark Higgs as well as the DM on the other, non-SM (*i.e.*, dark) brane with only the DP now living in the full 5-D bulk to communicate their existence to us. Thus, keeping (i) but with the breaking of $U(1)_D$ on the dark brane via the dark Higgs vev, we eliminate the need for KK excitations of the DM field while also disallowing any tree-level dark Higgs-SM Higgs mixing, and thus significantly diminishing the phenomenological role of the dark Higgs itself as we will see below. In what follows, we will separately consider and contrast both flat as well as the warped [20,21] versions of this setup in some detail assuming that the DM is a complex scalar field, ϕ , which does not obtain a vev. This choice, corresponding to a dominantly p-wave annihilation via the spin-1 DP mediator to SM fermions, allows us to trivially avoid the constraints from the CMB [22,23]. As we will see, in addition to the IR parameters noted above and suitably defined here in the 5-D context, only 2(3) additional parameters are present for the flat (warped) model version, these being the SM brane BLKT for the DP, τ , and size of the mass term, m_V . In the warped version, as is usual, the curvature of the anti-deSitter space scaled by the compactification radius, kR , is also, in principle, a free parameter. Here, however, the value of this quantity is roughly set by the ratio of the weak scale, ~ 250 GeV, to that associated with the DP mass, ~ 100 MeV, *i.e.*, $kR \sim 1.5 - 2$. In what follows, an $O(1)$ range of choices for the values of all of these quantities will be shown to directly lead to phenomenologically interesting results. Unlike in the previous setups, now the boundary conditions applied to wavefunction $v(y)$ will be significantly relaxed so that requirement of at least one of $v(y=0, \pi R) = 0$ is no longer a problem, and the values of these wavefunctions will be determined by the values of the parameters $m_V(\tau)$ on the dark (SM) brane.

The outline of this paper is as follows: In Section 2, we present the construction of this model while remaining agnostic to the specific geometry of the extra dimension, while in Section 3 we specialize our discussion to the case in which the extra dimension is flat and present a detailed analysis of this scenario. In Section 4, we present an analogous discussion of the model in the case of a warped extra dimension, with appropriate comparison to the results from the flat case scenario. Section 5 contains a summary and our conclusions.

2 General Setup Overview

Before beginning the analysis of the current setup, we will very briefly review the formalism from I that remains applicable, generalizing it slightly to incorporate either a flat or warped extra dimension. As noted in the Introduction, we consider the fifth dimension to be an interval $0 \leq y \leq \pi R$ bounded by two branes; for definiteness we assume that the SM is confined to the $y = 0$ brane whereas the DM and dark Higgs are constrained to the opposite brane at $y = \pi R$. For a flat extra dimension, this assignment of

branes is arbitrary, however we shall see that it has some physical motivation in the warped case. For now, we shall describe the metric as following the form,

$$ds^2 = f(y)^2 \eta_{\mu\nu} dx^\mu dx^\nu - dy^2, \quad (1)$$

where $f(y)$ is simply some function of the bulk coordinate y : For a flat extra dimension, $f(y) = 1$, while for an RS setup, $f(y) = e^{-ky}$, where k is a curvature scale. The DP, described by a gauge field $\hat{V}_A(x, y)$ lies in the full 5-D bulk, and kinetically mixes with the 4-D SM hypercharge gauge field $\hat{B}_\mu(x)$ on the SM brane via a 5-D KM parameter ϵ_5 as described (before symmetry breaking) by the action

$$S = \int d^4x \int_0^{\pi R} dy \left[-\frac{1}{4} (\hat{V}_{\mu\nu} \hat{V}^{\mu\nu} - 2f(y)^2 (\partial_\mu \hat{V}_y - \partial_y \hat{V}_\mu) (\partial^\mu \hat{V}^y - \partial^y \hat{V}^\mu)) \right. \\ \left. + \left(-\frac{1}{4} \hat{B}_{\mu\nu} \hat{B}^{\mu\nu} + \frac{\epsilon_5}{2c_w} \hat{V}_{\mu\nu} \hat{B}^{\mu\nu} + L_{SM} \right) \delta(y) \right], \quad (2)$$

where $c_w = \cos(\theta_w)$, the weak mixing angle, Greek indices denote only the 4-dimensional vector parts of the gauge field \hat{V} , and \hat{V}_y denotes the fifth component of this field. Here we see immediately that shifting the fields in the usual manner on the SM brane to remove the KM produces the small negative BLKT $\sim -\frac{\epsilon_5^2}{Rc_w^2}$ mentioned above. The presence of such a negative brane term is highly suggestive of the necessity of introducing a (larger) positive BLKT to the model (for example, in the case of a flat extra dimension, negative BLKT's such as this are well known to lead to tachyonic KK modes or ghost-like states). We shall later see more explicitly that such a positive BLKT is in fact necessary in both the cases of a warped and a flat extra dimension, working from the treatment of kinetic mixing in the effective 4-dimensional theory with an infinite tower of KK modes. Since spontaneous symmetry breaking takes place on the dark brane via the vev of the dark Higgs, S , we know [24, 25] that in the KK decomposition the 5th component of \hat{V}_A (which does not experience KM) and the imaginary part of S combine to form the Goldstone bosons eaten by \hat{V} to become the corresponding longitudinal modes. So, we are free in what follows to work in the $V_y = 0$ gauge, at least for the flat and Randall-Sundrum-like geometries that we are considering here. Then the alluded to the relevant KK decomposition for the 4-D components of \hat{V} is given by¹

$$\hat{V}^\mu(x, y) = \frac{1}{\sqrt{R}} \sum_{n=1}^{\infty} v_n(y) \hat{V}_n^\mu(x), \quad (3)$$

where we have factored out $R^{-1/2}$ in order to render $v_n(y)$ dimensionless. To produce a Kaluza-Klein tower, then we will require that the functions $v_n(y)$ must satisfy the equation of motion

$$\partial_y [f(y)^2 \partial_y v_n(y)] = -m_n^2 v_n(y) \quad (4)$$

in the bulk, where here the m_n are the physical masses of the various KK excitations. Defining the KK-level dependent quantity $\epsilon_n = \epsilon_5 v_n(y=0)$, which we see explicitly depends on the values of the DP KK wavefunctions evaluated on the SM brane, we see that the 5-D KM becomes an infinite tower of 4-D KM terms given by

$$\sum_n \frac{\epsilon_n}{2c_w} \hat{V}_n^{\mu\nu} \hat{B}_{\mu\nu}. \quad (5)$$

As discussed in I, the intuitive generalization of the usual kinetic mixing transformations, $\hat{B}^{\mu\nu} = B^{\mu\nu} + \sum_n \frac{\epsilon_n}{c_w} V_n^{\mu\nu}$, $\hat{V}^{\mu\nu} \rightarrow V^{\mu\nu}$, will be numerically valid in scenarios in which the infinite sum $\sum_n \epsilon_n^2 / \epsilon_1^2$ is approximately $\lesssim O(10)$, and $\epsilon_1 \ll 1$. Otherwise, terms of $O(\epsilon_1^2)$ (at least) become numerically significant and can't be ignored in the analysis, even if each individual ϵ_n remains small. In both the cases of a warped and flat extra dimension, the sum $\sum_n \epsilon_n^2 / \epsilon_1^2$ is within the acceptable range as long as there is a sufficiently large positive BLKT on the same brane as the SM-DP kinetic mixing, as was shown for flat space in I and will be demonstrated for warped space in Section 4. So, by selecting $\epsilon_1 \sim 10^{-(3-4)}$, within our present analysis we can always work to leading order in the ϵ_n 's, and thus the transformations $\hat{B}^{\mu\nu} = B^{\mu\nu} + \sum_n \frac{\epsilon_n}{c_w} V_n^{\mu\nu}$, $\hat{V}^{\mu\nu} \rightarrow V^{\mu\nu}$ will be sufficient for for our purposes in removing the KM. Finally

¹Note that $n = 1$ labels the lowest lying excitation appearing in this sum.

we note that the sum of the brane actions corresponding to the usual (positive) BLKT term for V on the SM brane and the corresponding dark Higgs generated mass term for V on the dark brane is given by

$$S_{branes} = \int d^4x \int_0^{\pi R} dy \left[-\frac{1}{4} V_{\mu\nu} V^{\mu\nu} \cdot \tau R \delta(y) + \frac{1}{2} m_V^2 R V_\mu V^\mu \delta(y - \pi R) \right]. \quad (6)$$

where factors of R have been introduced to make τ dimensionless as usual and for m_V to have the usual 4-D mass dimension. We note that one of the main advantages of our present setup is that the dark Higgs which generates the brane mass term m_V is isolated from any mixing with the SM Higgs, and as a result, its phenomenological relevance in this construction is quite limited. As such, for our analysis we can ignore this scalar and instead simply assume the existence of the brane-localized mass term m_V without further complications. We will define the 4-D gauge coupling of the DP to be that between the DM and the lowest V KK mode as evaluated on the dark brane. The action S_{branes} supplies the boundary conditions, as well as the complete orthonormality condition, necessary for the complete solutions of the v_n . These are

$$\left(f(0)^2 \partial_y + m_n^2 \tau R \right) v_n(0) = 0, \quad \left(f(\pi R)^2 \partial_y + m_n^2 R \right) v_n(\pi R) = 0 \quad (7)$$

for the boundary conditions, and

$$\frac{1}{R} \int_0^{\pi R} dy v_n(y) v_m(y) (1 + \tau R \delta(y)) = \delta_{nm} \quad (8)$$

for the orthonormality condition. At this point, once the function $f(y)$ is specified, as we shall do in Sections 3 and 4 for a flat and a warped extra dimension respectively, it is possible to uniquely determine the bulk wave functions $v_n(y)$ for all n given the parameters R , τ , m_V^2 , and whatever additional parameters are necessary to uniquely specify $f(y)$.

Beyond discussing characteristics of individual KK modes, we shall find it convenient at times in our analysis to speak in terms of summations over exchanges of the entire DP KK tower. In particular, the sum

$$F(y, y', s) \equiv \sum_n \frac{v_n(y) v_n(y')}{s - m_n^2} \quad (9)$$

shall appear repeatedly in our subsequent discussion, where for our purposes here s is simply a positive number, but in our actual analysis shall denote the Mandelstam variable of the same name. To evaluate this sum, we can perform an analysis similar to that of [25, 26]. First, we note that the orthonormality condition of the KK modes in Eq.(8) requires that

$$\begin{aligned} \frac{1}{R} \int_0^{\pi R} dy v_m(y) v_n(y) (1 + \tau R \delta(y)) &= \delta_{mn} \\ \rightarrow \sum_n v_n(y) v_n(y') (1 + \tau R \delta(y)) &= R \delta(y - y'), \end{aligned} \quad (10)$$

where the sum in the second line of this equation is over all KK modes n . We then note that the equation of motion Eq.(4) and the $y = 0$ boundary condition of Eq.(7) can be recast in an integral form as

$$v_n(y) = v_n(0) - m_n^2 \int_0^y dy_1 [f(y_1)]^{-2} \int_0^{y_1} dy_2 v_n(y_2) (1 + \tau R \delta(y_2)) \quad (11)$$

Using this integral form of the equation of motion for $v_n(y)$, we can now compute the sum $F(y, y', s)$. Combining Eqs.(10) and (11), we can write the integral equation

$$F(y, y', s) = \int_0^y dy_1 f(y_1)^{-2} \int_0^{y_1} dy_2 [R \delta(y_2 - y') - s F(y_2, y', s) (1 + \tau R \delta(y_2))] + F(0, y', s). \quad (12)$$

Eq.(12) can be straightforwardly rewritten as a differential equation,

$$\begin{aligned}\partial_y[f(y)^2 \partial_y F(y, y', s)] &= R\delta(y - y') - sF(y, y', s), \\ \partial_y F(y, y', s)|_{y=0} &= -s\tau Rf(0)^{-2}F(0, y', s), \\ \partial_y F(y, y', s)|_{y=\pi R} &= -m_V^2 Rf(\pi R)^{-2}F(\pi R, y', s),\end{aligned}\tag{13}$$

where the $y = 0$ boundary condition is explicitly in the integral equation Eq.(12), while the second is easily derivable from the $y = \pi R$ boundary condition on $v_n(y)$ given in Eq. (7). Once a function $f(y)$ (and therefore a metric) has been specified, the function $F(y, y', s)$ is then uniquely specified by Eq.(13).

With equations of motion for the KK modes' bulk profiles $v_n(y)$ and the summation $F(y, y', s)$ specified, it is now useful to discuss some general aspects of our construction's phenomenology before explicitly choosing a metric. First, we note that the effective couplings of the n^{th} KK mode of the DP to the DM on the dark brane are given by $g_n^{DM} = g_{5D}v_n(y = \pi R)/\sqrt{R}$, where g_{5D} is the 5-dimensional coupling constant appearing in the theory, while recalling that the effective kinetic mixing parameters ϵ_n are similarly given by $\epsilon_n = \epsilon_{5D}v_n(y = 0)/\sqrt{R}$. In terms of the value of these parameters for the least massive KK mode, $g_D \equiv g_1^{DM}$ and ϵ_1 , we can then write

$$\begin{aligned}g_n^{DM} &= g_D \frac{v_n(y = \pi R)}{v_1(y = \pi R)}, \\ \epsilon_n &= \epsilon_1 \frac{v_n(y = 0)}{v_1(y = 0)}.\end{aligned}\tag{14}$$

Armed with these relationships, our subsequent analysis will treat ϵ_1 , g_D , and the mass of the least massive KK DP excitation, m_1 (which we trade for R), as free parameters and identify them with the corresponding quantities that appear in the conventional 4-D KM portal model.

Finally, we also note that it is useful to give symbolic results for two cross sections that are of particular phenomenological interest for dark matter within the mass range we are considering, and which can be expressed in a manner agnostic to the specific functional form of the bulk wavefunctions $v_n(y)$ and the sum $F(y, y', s)$. First, we note that in the limit where the mass of the DM particle m_{DM} is far greater than the mass of an electron, we can approximate the DM-electron scattering cross section for direct detection as

$$\sigma_{\phi e} = 4\alpha_{\text{em}}m_e^2(g_D\epsilon_1)^2 \left| \frac{F(0, \pi R, 0)}{v_1(\pi R)v_1(0)} \right|^2.\tag{15}$$

To ensure that our DM candidate produces the correct relic abundance, we also must compute the thermally averaged annihilation cross section for DM into SM particles (which we shall denote by the symbol σ), weighted by the Møller velocity of the DM particle pair system $v_{M\phi l}$ in the cosmic comoving frame [27]. We are careful to note that σ here refers to the Lorentz-*invariant* cross section. To find this average, we must integrate $\sigma v_{M\phi l}$ weighted by the two Bose-Einstein energy distributions, $f(E)$, of the complex DM fields in the initial state. As noted in [27], if the freeze-out temperature, T_F satisfies $x_F = m_{DM}/T_F \gtrsim 3 - 4$ as it will below, we can approximate these Bose-Einstein distributions with Maxwell-Boltzmann ones, and can employ the following formula to express the thermal average as a one-dimensional integral,

$$\langle \sigma v_{M\phi l} \rangle = \frac{2x_F}{K_2^2(x_F)} \int_0^\infty d\varepsilon \varepsilon^{1/2} (1 + 2\varepsilon) K_1(2x_F\sqrt{1 + \varepsilon}) \sigma v_{lab},\tag{16}$$

where $K_n(z)$ denotes the modified Bessel function of the second kind of order n , v_{lab} is the relative velocity of the two DM particles in a frame in which one of them is at rest, and $\varepsilon \equiv (s - 4m_{DM}^2)/(4m_{DM}^2)$, *i.e.*, the kinetic energy per unit mass in the aforementioned reference frame. This integral can be performed numerically; in our numerical evaluations here we will assume $x_F = 20$ but note that other values in the 20-30 range give very similar results. We can proceed now by computing the cross-section for the annihilation of a DM particle-antiparticle pair into a pair of SM fermions of mass m_f and electric charge

Q_f , in which case we invoke the following expression for the cross-section of a $2 \rightarrow 2$ process,

$$\sigma v_{lab} = \frac{\sqrt{s(s-4m_f^2)}}{s(s-2m_{DM}^2)} \int \frac{d\Omega}{(64\pi^2)} |\mathcal{M}|^2, \quad (17)$$

where s is the standard Mandelstam variable, m_{DM} is the mass of the DM particle, Ω is the center-of-mass scattering angle and \mathcal{M} is the matrix element for the annihilation process we are considering. When s is far from any KK mode resonances, we arrive at the result

$$\sigma v_{lab} = \frac{1}{3} \frac{g_D^2 \epsilon_1^2 \alpha_{em} Q_f^2}{v_1(\pi R)^2 v_1(0)^2} \frac{(s+2m_f^2)(s-4m_{DM}^2) \sqrt{s(s-4m_f^2)}}{s(s-2m_{DM}^2)} |F(0, \pi R, s)|^2. \quad (18)$$

In practice, for both of the specific cases we shall consider in our analysis, we shall find it necessary to consider regions of parameter space such that DM annihilation through the first KK mode enjoys some resonant enhancement [28]. In order to accommodate this scenario, we have to modify Eq.(18) slightly, arriving at

$$\begin{aligned} \sigma v_{lab} = & \frac{1}{3} \frac{g_D^2 \epsilon_1^2 \alpha_{em} Q_f^2}{v_1(\pi R)^2 v_1(0)^2} \frac{(s+2m_f^2)(s-4m_{DM}^2) \sqrt{s(s-4m_f^2)}}{s(s-2m_{DM}^2)} \\ & \times \left| F(0, \pi R, s) - v_1(\pi R) v_1(0) \left(\frac{1}{s-m_1^2} - \frac{1}{s-m_1^2 + im_1 \Gamma_1} \right) \right|^2, \end{aligned} \quad (19)$$

where Γ_i is the total width of V_i which we need to calculate as a function of m_i . Physically, we have simply subtracted the contribution of the lowest-lying KK mode from the sum $F(0, \pi R, s)$, where its propagator appears with its pole mass, and added this contribution again with the Breit-Wigner mass instead. Since the annihilation of two complex scalars into a pair of fermions through a vector gauge boson is p -wave process, and so is v_{rel}^2 suppressed at later times (*i.e.*, at lower temperatures when the DM is moving slowly), we are safe from the previously mentioned strong constraints on DM annihilation during the CMB at $z \sim 10^3$ [23]. We further note that if $m_{DM} > m_1$, then we would expect the s -wave process $\phi\phi^\dagger \rightarrow 2V_1$ to be dominant for unsuppressed values of g_D . In order to avoid this possibility, we must then require that $m_{DM} < m_1$ and this will be reflected in our considerations below. We note that if $m_1 > 2m_{DM}$ then the $O(g_D^2)$ decay $V_1 \rightarrow \phi\phi^\dagger$ will dominate, otherwise, V_1 will decay to SM fermions with a suppressed $O(e^2 \epsilon_1^2)$ decay partial width.

It should be noted that in computing the cross sections of Eqs.(15) and (19), we have treated the system as though *all* KK tower members couple to the SM like normal dark photons, namely, V_n couples to SM fermions with a coupling strength of $eQ\epsilon_n$. As noted in I, this is not strictly true: If the full computation for the various model couplings is done, the DP coupling of the n^{th} KK mode to SM fermions is only well-approximated by this expression if m_n , the KK mode's mass, is much less than the mass of the Z boson, which if we sum over the entire infinite tower of KK modes breaks down for sufficiently large n . However, numerically we find that the cross sections in Eqs.(15) and (19) are heavily dominated by exchanges of the lighter KK modes in which this approximation is valid, rather than the exchanges of the heavier modes with $m_n \gtrsim m_Z$ for which the approximation breaks down. Similarly, the dominance of the lighter KK modes with $m_n \ll m_Z$ in these cross sections numerically overwhelms the contribution from Z boson exchanges, even though the Z boson also possesses non-zero couplings to both the SM and DM fields once mixing is fully accounted for.

3 Flat Space Model Setup

In order to further explore the phenomenology of our construction, we must now specify the geometry of the extra dimension, namely by selecting a specific function $f(y)$ in Eq.(1). With this determined, we can then straightforwardly find the spectrum of KK gauge bosons V_n , their bulk wavefunctions $v_n(y)$,

and concrete expressions for the cross sections of Eqs.(15) and (19). Initially, we shall consider the case of a flat extra dimension, *i.e.*, $f(y) = 1$. The equation of motion for the bulk profile $v_n(y)$ is then straightforward; from the generic case given in Eqs.(4) and (7), we quickly arrive at

$$\begin{aligned} \partial_y^2 v_n(y) &= -m_n^2 v_n(y), \\ (\partial_y + m_n^2 \tau R) v_n(y)|_{y=0} &= 0, \\ (\partial_y + m_n^2 R) v_n(y)|_{y=\pi R} &= 0. \end{aligned} \tag{20}$$

which when combined with the orthonormality condition Eq.(8) quickly yields the expressions

$$\begin{aligned} v_n(y) &= A_n (\cos(x_n^F(y/R)) - \tau x_n^F \sin(x_n^F(y/R))), \\ A_n &\equiv \sqrt{\frac{2}{\pi}} \left(1 + (x_n^F \tau)^2 + (1 - (x_n^F \tau)^2) \frac{\sin(2\pi x_n^F)}{2\pi x_n^F} + \frac{2\tau}{\pi} \cos^2(\pi x_n^F) \right)^{-\frac{1}{2}}, \\ x_n^F &\equiv m_n R, \quad a_F \equiv m_V R, \end{aligned} \tag{21}$$

where we have defined the dimensionless quantities x_n^F and a_F from combinations of dimensionful parameters for the sake of later convenience². The allowed values of x_n^F (and hence the mass spectrum of the KK tower) are given by the solutions to the equation,

$$\tan(\pi x_n^F) = \frac{(a_F^2 - (x_n^F)^2 \tau)}{x_n^F (1 + a_F^2 \tau)}. \tag{22}$$

Given the results of Eqs.(21) and (22), we can now examine the behavior of a number of phenomenologically relevant quantities. To begin, it is useful to get a feel for the numerics of x_1^F , the lowest-lying root of the mass eigenvalue equation Eq.(22). Since we are free to choose m_1 within the $\sim 0.1 - 1$ GeV mass range of interest, the lowest root $x_1^F = m_1 R$ tells us the value of the compactification radius R within this setup, hence, the value of $x_1^F(a_F, \tau)$ is important to consider. In I, where boundary conditions were used to break $U(1)_D$, the parameter a_F is, of course, absent. However, it was found that x_1^F in that case was a decreasing function of τ , as is typical for the effect of BLKs, with $x_1^F(\tau = 0) = 1/2$. Here, on the other hand, it is the value of $a_F \neq 0$ that generates a mass for the lowest lying DP KK state so that we expect $x_1^F \rightarrow 0$ as $a_F \rightarrow 0$ and thus to grow with increasing a_F . The top and bottom panels of Fig. 1 show that, indeed, the values of x_1^F follow this anticipated behavior. For a fixed value of a_F , x_1^F decreases as τ increases and for a fixed value of τ , x_1^F increases with the value of a_F .

Beyond the position of the lowest-lying root of Eq.(22), the particular spectrum of the more massive KK modes are obviously of significant interest. A clear phenomenological signal for the types of models we are considering is the experimental observation of the DP KK excitations, perhaps most importantly that of the second DP KK excitation. Hence, knowing where the ‘next’ state beyond the lowest lying member of the KK tower may lie is of a great deal of importance, *i.e.*, where do we look for the DP KK excitations if the lowest KK state is discovered? In Fig. 2 we display the ratio $m_2/m_1 = x_2^F/x_1^F$ as a functions of a_F, τ and we see that for a reasonable variation of these parameters this mass ratio lies in the range 3 – 4. Note that for fixed a_F this ratio increases with increasing τ (mostly since since x_1^F is pushed lower). Meanwhile, for any fixed value of τ , this ratio sharply declines with increasing a_F in the region $a_F \lesssim 1$ (largely because x_1^F itself decreases sharply in this regime), while for $a_F \gtrsim 1$ the ratio slowly increases with increasing a_F . Non-zero values of a_F, τ particularly influence the low mass end of the DP KK mass spectrum as, *e.g.*, $a_F \neq 0$ provides the mass for the lightest KK mode in the present case. However, beyond the first few KK levels the masses of the DP KK states, in particular the ratio m_n/m_1 grows roughly linearly with increasing n with a slope that is dependent on the values of the parameters a_F, τ as is shown in Fig. 3. It is actually straightforward to see the eventual linear trend of the lines in Fig. 3 analytically, using the root equation Eq.(22). In particular, note that as $x_n^F \rightarrow \infty$,

²The label “F” is used here to distinguish these flat space results from those of the warped case which we will discuss further below.

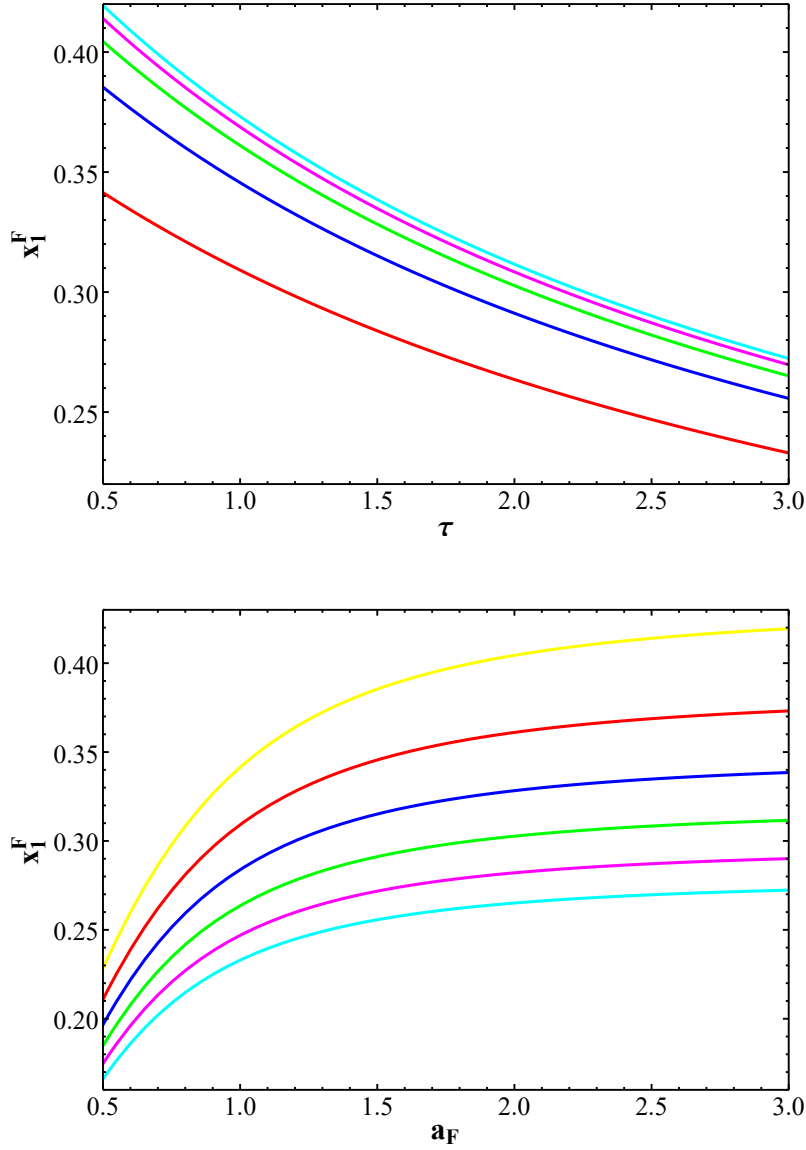


Figure 1: (Top) Value of the root x_1^F as a function of τ for, from bottom to top, $a_F = 1, 3/2, 2, 5/2$ and 3 , respectively. (Bottom) Value of the root x_1^F as a function of a_F for, from top to bottom, $\tau = 1/2, 1, 3/2, 2, 5/2$ and 3 , respectively.

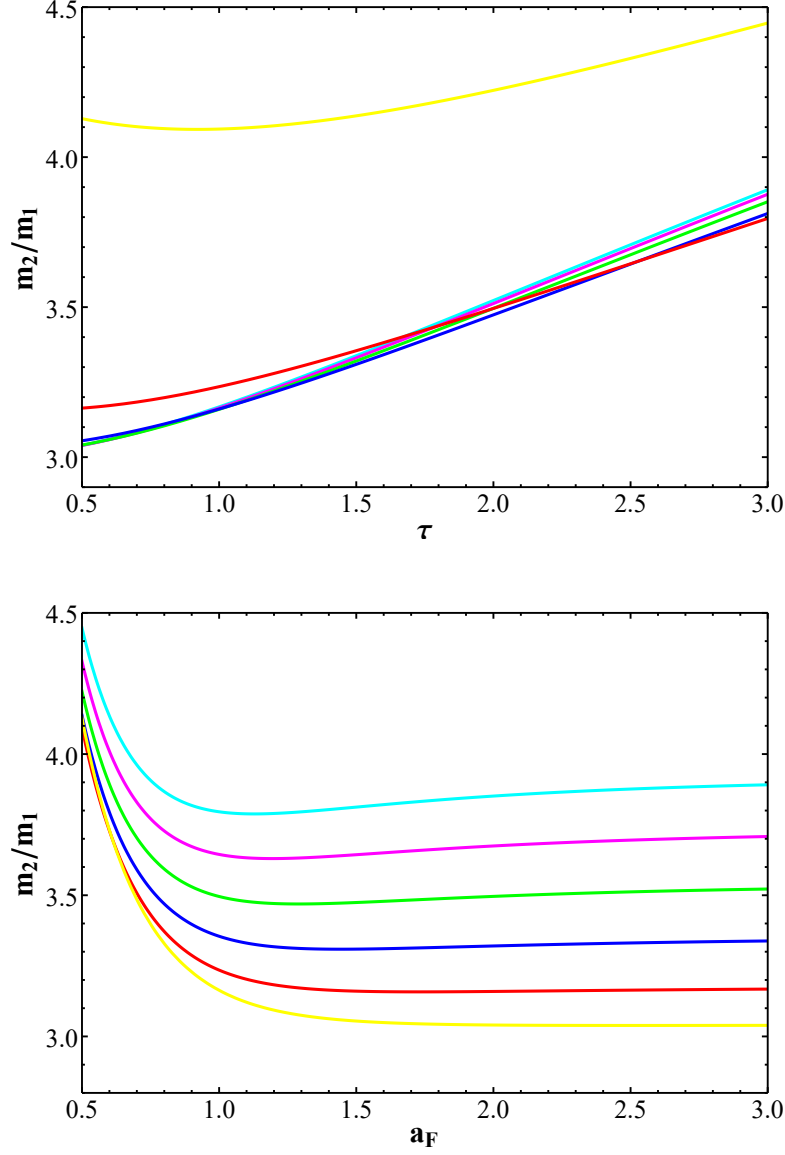


Figure 2: (Top) The mass ratio of the lowest two DP KK states, $m_2/m_1 = x_2^F/x_1^F$, as a function of τ for $a_F = 3$ (cyan), $5/2$ (magenta), 2 (green), $3/2$ (blue), 1 (red), and $1/2$ (yellow), respectively. (Bottom) As in the previous panel, but now as a function of a_F assuming $\tau = 3$ (cyan), $5/2$ (magenta), 2 (green), $3/2$ (blue), 1 (red), and $1/2$ (yellow), respectively.

Eq.(22) approaches

$$\text{tanc}(\pi x_n^F) = -\frac{\tau}{\pi(1+a_F^2\tau)}, \quad (23)$$

where $\text{tanc}(z) \equiv \tan(z)/z$. It is well known that the difference between consecutive solutions of $\text{tanc}(z) = C$, for some constant C , approaches π for very large z . So, we can see that for high-mass KK modes, the difference between consecutive solutions of Eq.(22) will approach 1. Hence, the slope of the lines in Fig. 3 can be easily approximated as $\sim (x_1^F)^{-1}$, and will therefore exhibit the inverse of the dependence of x_1^F on the parameters τ and a_F , which we have already observed in Fig. 1. In addition, we can note that without taking the ratio of x_n^F to x_1^F , any large- n solution of Eq.(22) eventually follows the pattern $x_n^F \approx n$.

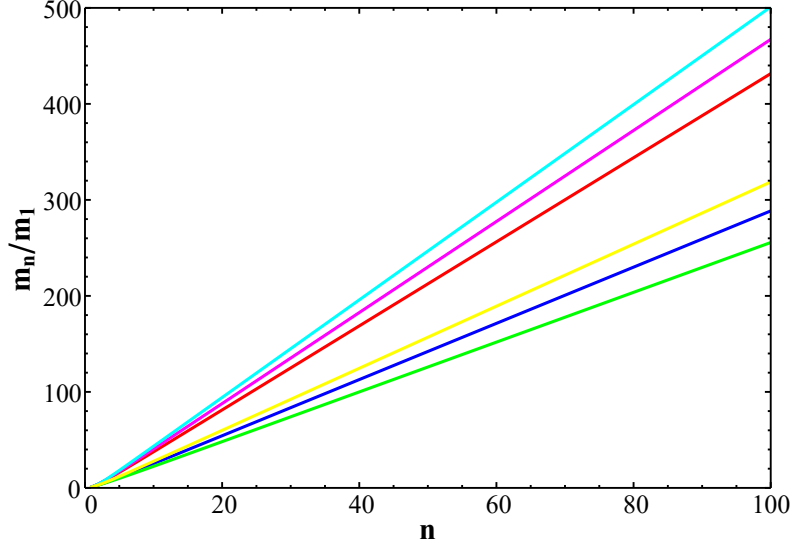


Figure 3: Approximate linear growth of the relative DP KK mass ratio m_n/m_1 as a function of n for various choices of $(\tau, a_F) = (1/2, 1/2)$ [red], $(1/2, 1)$ [blue], $(1/2, 3/2)$ [green], $(1, 1/2)$ [magenta], $(3/2, 1/2)$ [cyan] and $(1, 1)$ [yellow], respectively.

The next quantities of phenomenological relevance are the relative values of the KM parameters, ϵ_n/ϵ_1 , and the couplings of the DP KK tower states to DM, g_{DM}^n/g_D ; note that these latter quantities are found to oscillate in sign. Before exploring the numerics in detail here, it is useful to note that one can get a feel for the behavior of these ratios by purely analytical methods. In particular, by invoking Eqs.(14),(21), and (22), it is possible to derive the expressions

$$\begin{aligned} \left(\frac{\epsilon_n}{\epsilon_1}\right)^2 &= \left(\frac{a_F^4 + (x_n^F)^2}{a_F^4 + (x_1^F)^2}\right)\lambda_F, \\ \left(\frac{g_{DM}^n}{g_D}\right)^2 &= \left(\frac{(1 + (x_n^F)^2\tau^2)(x_n^F)^2}{(1 + (x_1^F)^2\tau^2)(x_1^F)^2}\right)\lambda_F, \\ \lambda_F &\equiv \frac{\pi(1 + (x_1^F)^2\tau^2)(a_F^4 + (x_1^F)^2) + (1 + a_F^2\tau)(a_F^2 + (x_1^F)^2\tau)}{\pi(1 + (x_n^F)^2\tau^2)(a_F^4 + (x_n^F)^2) + (1 + a_F^2\tau)(a_F^2 + (x_n^F)^2\tau)}. \end{aligned} \quad (24)$$

From Eq.(24), we can readily take the limits of $(\epsilon_n/\epsilon_1)^2$ and $(g_{DM}^n/g_D)^2$ at large n (and hence large

$x_n^F \approx n$). We arrive at the result that as $n \rightarrow \infty$

$$\begin{aligned} \left(\frac{\epsilon_n}{\epsilon_1}\right)^2 &\rightarrow \frac{\pi(1+(x_1^F)^2\tau^2)(a_F^4+(x_1^F)^2)+(1+a_F^2\tau)(a_F^2+(x_1^F)^2\tau)}{\pi\tau^2(a_F^4+(x_1^F)^2)}\frac{1}{n^2}, \\ \left(\frac{g_{DM}^n}{g_D}\right)^2 &\rightarrow \frac{\pi(1+(x_1^F)^2\tau^2)(a_F^4+(x_1^F)^2)+(1+a_F^2\tau)(a_F^2+(x_1^F)^2\tau)}{\pi(1+(x_1^F)^2\tau^2)(x_1^F)^2}. \end{aligned} \quad (25)$$

From the first expression in Eq.(25), we see that the ratio (ϵ_n/ϵ_1) falls roughly as $1/n$ for large n ; this result is readily borne out numerically in the top panel of Fig. 5, where we also see that even for small n , ϵ_n never significantly exceeds the value of ϵ_1 , offering encouraging evidence that the small-KM limit we took in Section 2 was valid. More rigorously demonstrating this validity, however, will require the use of sum identities we shall derive later in this section.

In contrast to the behavior of the effective kinetic mixing terms ϵ_n/ϵ_1 , the ratio $|g_{DM}^n/g_D|$ approaches a constant non-zero value as $n \rightarrow \infty$. The precise value of this asymptotic limit of the ratio $|g_{DM}^n/g_D|$ is naturally of quite significant phenomenological interest: If $|g_{DM}^n/g_{DM}|$ is large, one might be concerned that even for a reasonable value of $g_D \lesssim 1$, the DM particle may experience some non-perturbative couplings to the various KK modes.³ In Fig. 4, we explore the τ and a_F dependence of this asymptotic coupling limit numerically; notably, we find that the coupling ratio increases sharply as a_F increases. For comparison's sake, in both panels of Fig. 4, we have depicted as a dashed line the *maximum* $|g_{DM}^n/g_D|$ that would be allowed such that all couplings would remain perturbative (that is, have a structure constant $(g_{DM}^n)^2/(4\pi) < 1$) given a choice of $g_D = 0.3$, that is, assuming that the coupling of DM to the first KK mode of the dark photon field has approximately the same coupling constant as the electroweak force. In the figure then, we see that such a choice of g_D is only permitted when $a_F \lesssim 3/2$; much larger and the DM interactions with large- n KK modes become strongly coupled. In both Figs. 4 and 5, however, we see that limiting our choice of a_F to $a_F \lesssim 3/2$ leads to substantially more modest asymptotic values of $|g_{DM}^n/g_D|$, of $\lesssim 10$. Because $|g_{DM}^n/g_D|$ rises quadratically (or more accurately, the square of this ratio rises quartically) with increasing a_F , these conditions would be only slightly less restrictive if a somewhat smaller value of g_D , *e.g.*, $g_D = 0.1$ were chosen.

To continue our discussion of the phenomenology of our construction, we must now also find the sum $F(y, y', s)$, which we remind the reader is defined in Eq.(9), for the flat space τ case, which we can accomplish by inserting $f(y) = 1$ into Eq.(13), yielding

$$\begin{aligned} \partial_y^2 F(y, y', s) &= R\delta(y - y') - sF(y, y', s), \\ \partial_y F(y, y', s)|_{y=0} &= -s\tau RF(0, y', s), \\ \partial_y F(y, y', s)|_{y=\pi R} &= -m_V^2 RF(\pi R, y', s), \end{aligned} \quad (26)$$

from which the solution

$$F(y, y', s) = R^2 \frac{[\cos(\sqrt{s}y_{<}) - R\sqrt{s}\sin(\sqrt{s}y_{<})][\sqrt{s}R\cos(\sqrt{s}(y_{>} - \pi R)) - a_F^2\sin(\sqrt{s}(y_{>} - \pi R))]}{R\sqrt{s}(-a_F^2 + sR^2\tau)\cos(\pi R\sqrt{s}) + sR^2(1 + a_F^2\tau)\sin(\pi R\sqrt{s})}, \quad (27)$$

$$y_{>} \equiv \max(y, y'), \quad y_{<} \equiv \min(y, y')$$

can be straightforwardly derived. We see that, as expected, the sum $F(y, y', s)$ has poles whenever $s = m_n^2$, as can be seen from the mass eigenvalue condition Eq.(22); in other words, our sum of propagators possesses poles exactly where the individual propagators have poles. Additionally, equipped with this sum, it is possible to derive in closed form the sum $\sum_n \epsilon_n^2/\epsilon_1^2$, which we recall from I and Section 2 must be $\lesssim 10$ in order for our assumption of small KM to be valid. Taking the limit of $F(y, y', s)$ as $s \rightarrow 0$, we arrive at the result

$$-F(y, y', 0) = \sum_n \frac{v_n(y)v_n(y')}{m_n^2} = R^2 \left(\frac{1}{a_F^2} + \pi \right) - \theta(y - y')Ry - \theta(y' - y)Ry'. \quad (28)$$

³We also note that a large $|g_{DM}^n/g_{DM}|$ may raise concerns about non-convergence of various sums over all KK modes, such as those that appear in Eqs.(15) and (19), however, as we shall see later in this section, these sums remain well-defined.

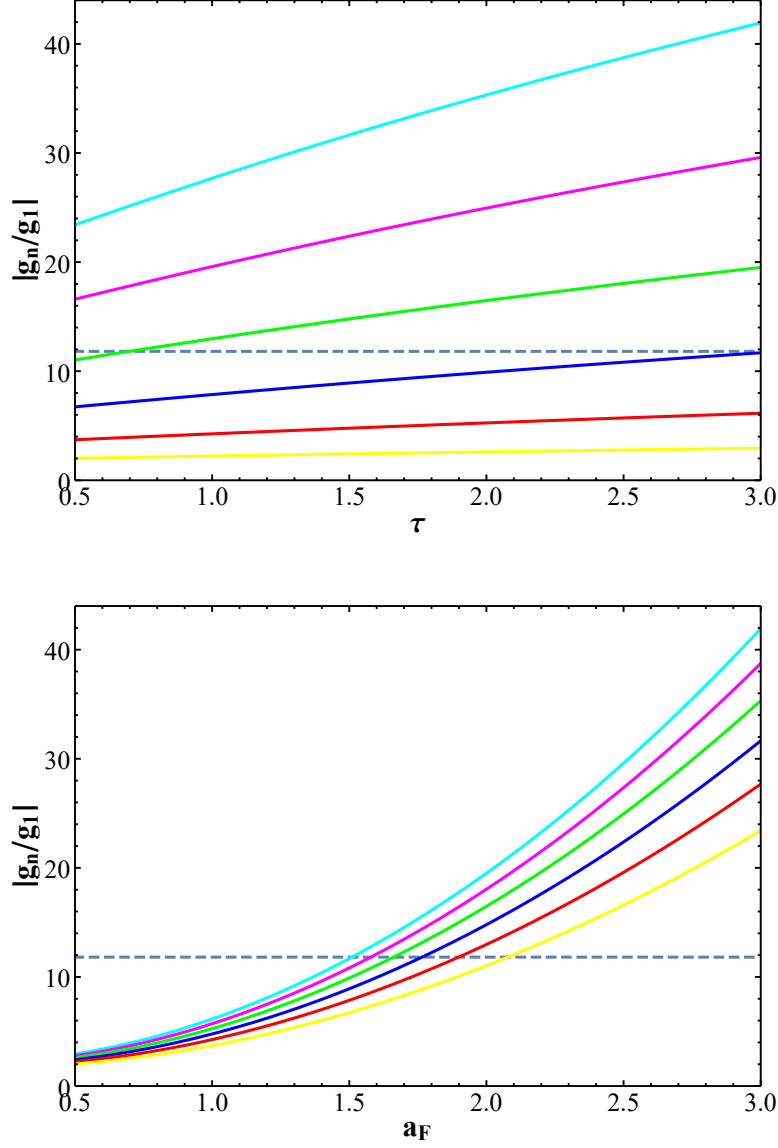


Figure 4: (Top) The limit of the ratio $|g_{DM}^n/g_D|$ as $n \rightarrow \infty$, as a function of τ for $a_F = 3$ (cyan), $5/2$ (magenta), 2 (green), $3/2$ (blue), 1 (red), and $1/2$ (yellow), respectively. The dashed line denotes the largest possible ratio such that the couplings of the DM particle to the gauge boson KK modes remain perturbative for all KK modes in the theory, assuming $g_D = 0.3$ (Bottom) As in the previous panel, but now as a function of a_F assuming $\tau = 3$ (cyan), $5/2$ (magenta), 2 (green), $3/2$ (blue), 1 (red), and $1/2$ (yellow), respectively.

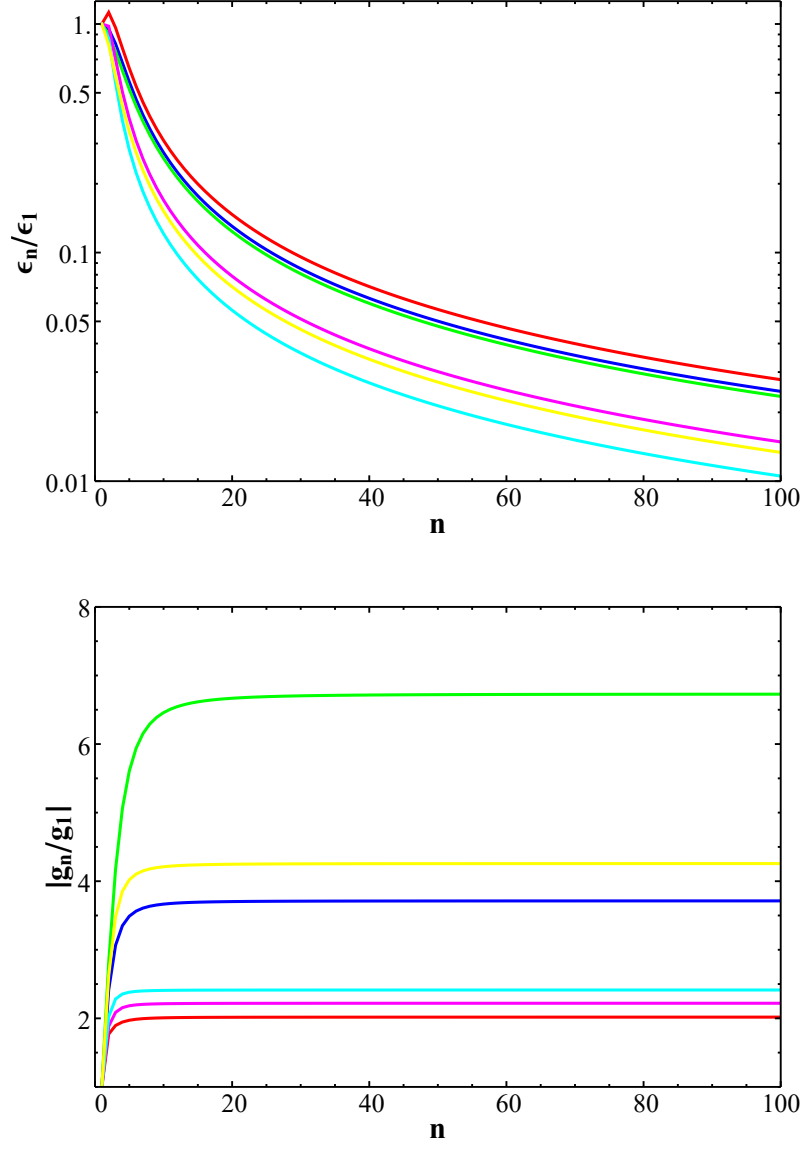


Figure 5: (Top) The ratio ϵ_n/ϵ_1 as a function of n for various choices of $(\tau, a_F) = (1/2, 1/2)$ [red], $(1/2, 1)$ [blue], $(1/2, 3/2)$ [green], $(1, 1/2)$ [magenta], $(3/2, 1/2)$ [cyan], and $(1, 1)$ [yellow], respectively. (Bottom) Same as the top panel but now for the absolute value of the strength of the n^{th} KK coupling of the DP to DM in units of g_D . Note that this quantity alternates in sign.

Differentiating this sum with respect to y at $y = 0$ and applying the SM-brane boundary condition given in Eq.(20), we rapidly arrive at

$$\begin{aligned} \sum_n v_n(0)^2 &= \frac{1}{\tau} \\ \rightarrow \sum_n \frac{\epsilon_n^2}{\epsilon_1^2} &= \sum_n \frac{v_n(0)^2}{v_1(0)^2} = \frac{1}{\tau v_1(0)^2}. \end{aligned} \quad (29)$$

The form of the sum in the second line of Eq.(29) already then confirms what has previously been observed in I, namely, that a nontrivial positive BLKT is necessary for the consistency of our KM analysis. The sum sharply increases to infinity as $\tau \rightarrow 0$, indicating that an insufficiently large τ will result in the sum being unacceptably large, namely $\gtrsim O(10)$. Furthermore, a *negative* τ would suggest a still more worrying scenario, indicating the need for at least one KK state to be ghost-like (have a negative norm squared). To determine if our kinetic mixing treatment is valid for the full parameter space we consider, we depict the sum $\sum_n \epsilon_n^2/\epsilon_1^2$ in Fig. 6. Our results here explicitly confirm those observed in I, namely, that for selections of (τ, a_F) such that $\tau \gtrsim 1/2$, the summation $\sum_n \epsilon_n^2/\epsilon_1^2$ remains small enough not to vitiate our treatment of kinetic mixing: The sum remains $\lesssim O(10)$.

Next, we apply the results of Eqs.(21), (22), and (27) to find the DM- e^- scattering cross section, to explore the possibility of direct detection of the DM. Inserting Eq.(27) into Eq.(15) yields

$$\begin{aligned} \sigma_{\phi e} &= \frac{4\alpha_{em}m_e^2(g_D\epsilon_1)^2 R^4}{v_1(0)^2 v_1(\pi R)^2 a_F^4} \\ &= \frac{4\alpha_{em}m_e^2(g_D\epsilon_1)^2 (x_1^F)^4}{v_1(0)^2 v_1(\pi R)^2 m_1^4 a_F^4}, \end{aligned} \quad (30)$$

where in the second line we have substituted the parameter m_1 , the mass of the lowest-lying KK mode of the dark photon field, for the compactification radius R . We can now suggestively rewrite this expression as

$$\begin{aligned} \sigma_{\phi e} &= (2.97 \times 10^{-40} \text{ cm}^2) \left(\frac{100 \text{ MeV}}{m_1} \right)^4 \left(\frac{g_D \epsilon_1}{10^{-4}} \right)^2 \Sigma_{\phi e}^F, \\ \Sigma_{\phi e}^F &\equiv \frac{(x_1^F)^4}{v_1(0)^2 v_1(\pi R)^2 a_F^4} = \left| \sum_{n=0}^{\infty} \frac{(x_1^F)^2 v_n(0) v_n(\pi R)}{(x_n^F)^2 v_1(0) v_1(\pi R)} \right|^2. \end{aligned} \quad (31)$$

Note here that the quantity $\Sigma_{\phi e}^F$ depends *only* on the model parameters (τ, a_F) , while the rest of the expression above is independent of them. While the closed form of $\Sigma_{\phi e}^F$ is convenient for calculation, we have also included an explicit expression for this quantity in terms of an infinite sum over KK modes—*notably*, because the quantity $g_{DM}^n \epsilon_n$ (or alternatively, $v_n(\pi R) v_n(0)$) alternates in sign and decreases sharply with increasing n , we can see in Fig. 7 that the sum rapidly converges, coming within $O(10^{-2})$ corrections to the value of the closed form of $\Sigma_{\phi e}^F$ even when the sum is truncated at $n = 10$.

Looking at the numerical coefficient of $\Sigma_{\phi e}^F$ in Eq.(31), meanwhile, we see that for $m_1 \sim O(100 \text{ MeV})$ and $g_D \epsilon_1 \sim 10^{-4}$, the DM- e^- scattering cross section easily avoids current direct detection constraints as long as the quantity $\Sigma_{\phi e}^F$ is $O(1)$ or smaller [29–31], although it does lie within the possible reach of future experiments such as SuperCDMS [31]. We can see that this is the case for a broad range of parameters in Fig. 8; for every choice of (τ, a_F) that we are considering here, $\Sigma_{\phi e}^F$ lies between 0.6 and 0.9 implying that the KK states lying above the lightest one do not make critical contributions to this cross section. Hence, at present, this model can easily evade present DM direct detection constraints for reasonable choices of $m_1 \sim 100 \text{ MeV}$ and $g_D \epsilon_1 \sim 10^{-4}$.

Our brief phenomenological survey of the flat space scenario now concludes with a discussion of the thermally averaged annihilation cross section at freeze-out, that is, demonstrating that this construction is capable of producing the correct relic density of DM in the universe. To begin, we insert Eq.(27) into the expression for the $\phi^\dagger \phi \rightarrow f \bar{f}$ (where f is some fermion species) velocity-weighted annihilation cross

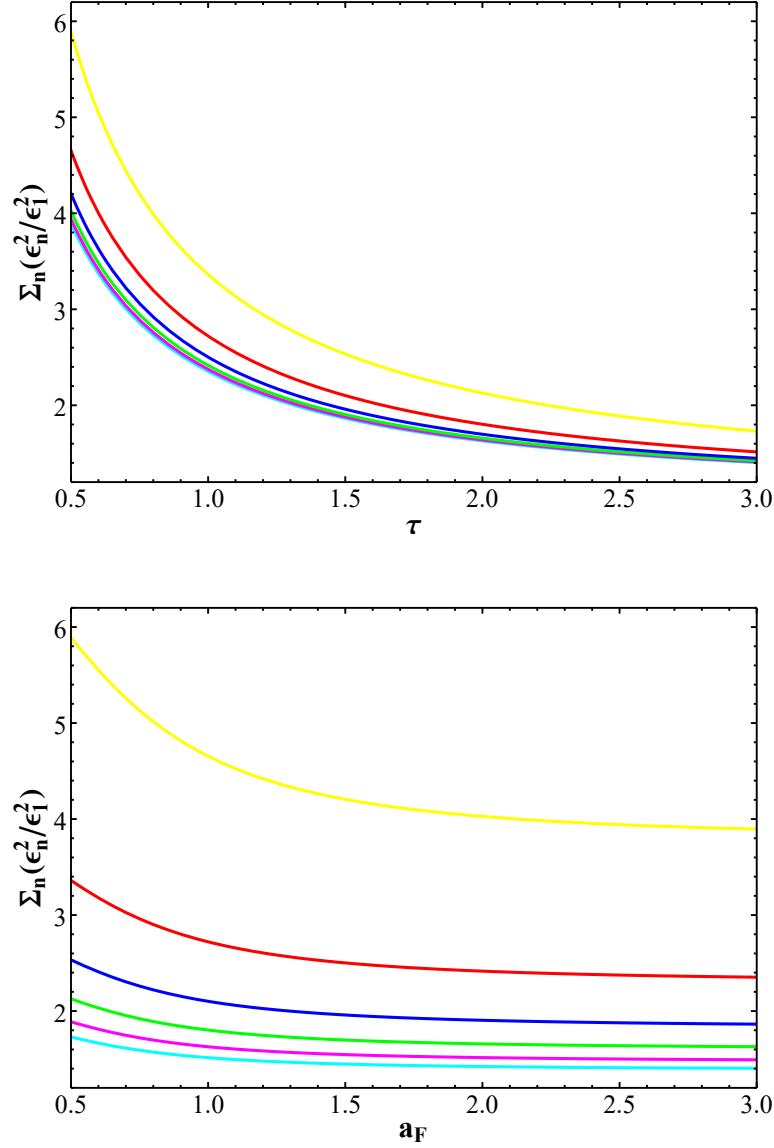


Figure 6: (Top) The sum $\sum_n \epsilon_n^2 / \epsilon_1^2$ over all n , as a function of τ for $a_F = 3$ (cyan), $5/2$ (magenta), 2 (green), $3/2$ (blue), 1 (red), and $1/2$ (yellow), respectively. (Bottom) As in the previous panel, but now as a function of a_F assuming $\tau = 3$ (cyan), $5/2$ (magenta), 2 (green), $3/2$ (blue), 1 (red), and $1/2$ (yellow), respectively.

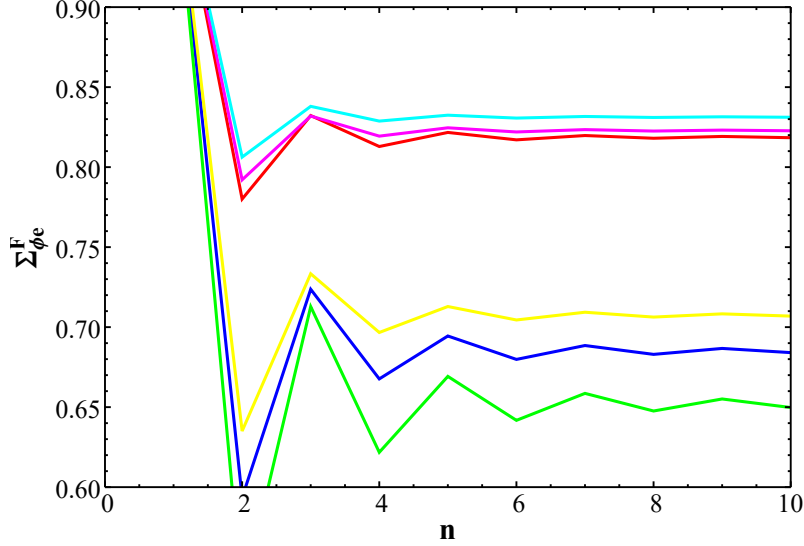


Figure 7: The explicit KK sum form of $\Sigma_{\phi_e}^F$, defined in Eq.(31), where only terms coming from the first n KK modes are included in the sum, for the choices of $(\tau, a_F) = (1/2, 1/2)$ [red], $(1/2, 1)$ [blue], $(1/2, 3/2)$ [green], $(1, 1/2)$ [magenta], $(3/2, 1/2)$ [cyan] and $(1, 1)$ [yellow], respectively.

section of Eq.(19). This yields the result

$$\begin{aligned} \sigma_{v_{lab}} &= \frac{1}{3} \frac{g_D^2 \epsilon_1^2 \alpha_{em} Q_f^2}{v_1(\pi R)^2 v_1(0)^2} \frac{(s + 2m_f^2)(s - 4m_{DM}^2) \sqrt{s(s - 4m_f^2)} R^4}{s(s - 2m_{DM}^2)} \\ &\times \left| \frac{1}{R^2} F(0, \pi R, s) - \frac{v_1(\pi R)v_1(0)}{sR^2 - (x_1^F)^2} + \frac{v_1(\pi R)v_1(0)}{sR^2 - (x_1^F)^2 + i(x_1^F)R\Gamma_1} \right|^2, \\ \frac{1}{R^2} F(0, \pi R, s) &= \frac{1}{(-a_F^2 + sR^2\tau) \cos(\pi R\sqrt{s}) + R\sqrt{s}(1 + a_F^2\tau) \sin(\pi R\sqrt{s})}. \end{aligned} \quad (32)$$

We can then use this expression in the single integral formula for a thermally averaged annihilation cross section given in Eq.(16), and compare the results to the approximate necessary cross section to reproduce the (complex) DM relic density with a p -wave annihilation process, namely $\simeq 7.5 \times 10^{-26} \text{ cm}^3/\text{s}$ [32]. We note that this quantity is the *only* one in our analysis which has any direct dependence on the mass of the DM, m_{DM} , (assuming, as we do, that the DM particle's mass is substantially greater than that of the electron). In fact, because we must rely on resonant enhancement in order to achieve the correct relic density, we see that with all the other parameters fixed our results for the thermally averaged cross section are extremely sensitive to m_{DM} and largely agnostic to differing choices of (τ, a_F) . In Fig. 9, we depict the thermally averaged velocity-weighted cross section as a function of the DM mass m_{DM} , requiring, as we have argued must be the case in Section 2, that $m_{DM} < m_1$. For demonstration purposes, we have selected that $m_1 = 100 \text{ MeV}$, $x_F = m_{DM}/T = 20$, $g_D = 0.3$, $(g_D \epsilon_1) = 10^{-4}$, and have included only the possibility of the DM particles annihilating into an e^+e^- final state.

Notably, the cross sections depicted are largely independent of the choices of (τ, a_F) near values of m_{DM}/m_1 that produce the correct relic abundance (that is, relatively near the m_1 resonance of the cross section). In fact, for *all* parameter space points we depict here, it is possible to produce the correct cross section when $m_{DM} \sim 0.36m_1$ or $m_{DM} \sim 0.54m_1$; however, other values would be required if we

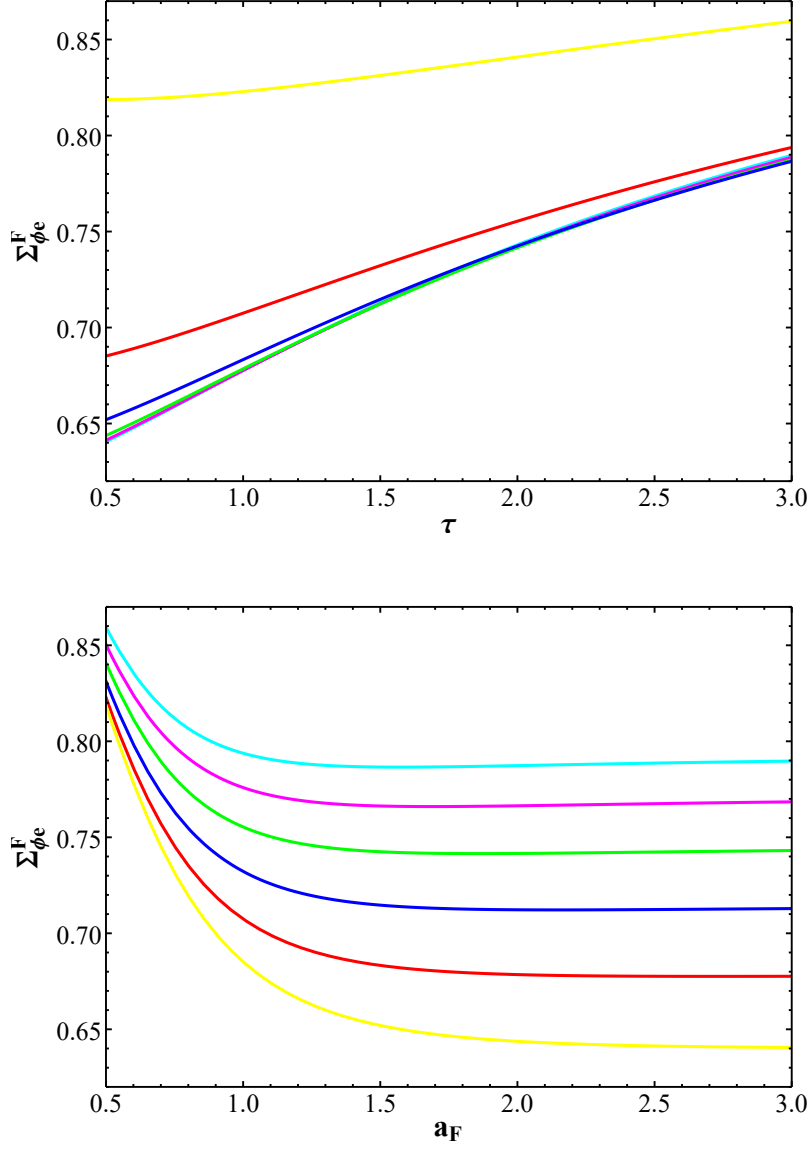


Figure 8: (Top) The sum $\Sigma_{\phi_e}^F$, defined in Eq.(31), as a function of τ for $a_F = 3$ (cyan), $5/2$ (magenta), 2 (green), $3/2$ (blue), 1 (red), and $1/2$ (yellow), respectively. (Bottom) As in the previous panel, but now as a function of a_F assuming $\tau = 3$ (cyan), $5/2$ (magenta), 2 (green), $3/2$ (blue), 1 (red), and $1/2$ (yellow), respectively.

also varied m_1 or $g_D \epsilon_1$. By leveraging the resonance, therefore, our model is clearly able to reproduce the observed relic abundance for a wide variety of reasonable points in parameter space.

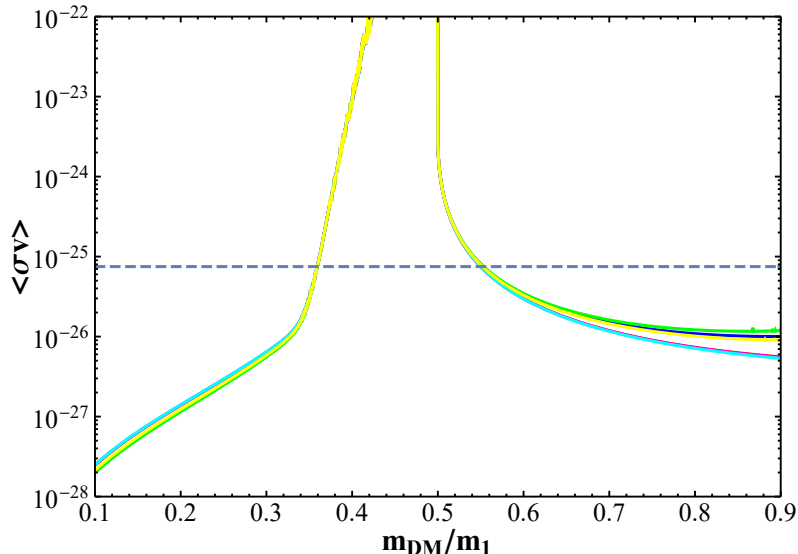


Figure 9: The thermally averaged, velocity-weighted cross section in cm^3/s for the annihilation process $\phi^\dagger \phi \rightarrow f \bar{f}$, where the final-state fermions f are electrons where only terms coming from the first n KK —TR n ? modes are included in the sum, for the choices of $(\tau, a_F) = (1/2, 1/2)$ [red], $(1/2, 1)$ [blue], $(1/2, 3/2)$ [green], $(1, 1/2)$ [magenta], $(3/2, 1/2)$ [cyan] and $(1, 1)$ [yellow], respectively. The dashed line denotes the value for this cross section necessary to produce the observed relic abundance of DM after freeze out.

4 Warped Space Model Analysis

We now consider the possibility that the extra dimension is not flat, but rather has a Randall-Sundrum-like geometry with a curvature scale k . In this case, $f(y)$ in the metric of Eq.(1) shall be e^{-ky} , but our analysis closely follows that of the flat space scenario. The warped geometry does, however, necessitate additional care in certain aspects of model construction, which we should address before moving forward with our discussion.

First, in the warped space scenario, because $f(y)$ is non-trivial, we need two parameters to describe the metric rather than the single parameter, R , that we used in the flat-space analysis. We shall find the most convenient parameters with which to describe our metric are kR , the product of the curvature scale and the compactification radius, and the so-called “KK mass”, $M_{KK} \equiv k \exp(-kR\pi)$. Second, unlike the flat-space case, our choice to place the SM on the $y = 0$ brane and the DM on the $y = \pi R$ brane is no longer arbitrary. Specifically, we note that naturalness suggests that $\sim M_{KK}$ is a natural scale for mass terms localized on the $y = \pi R$ brane, and that the lowest-mass Kaluza-Klein modes of any bulk fields should also in general be $O(M_{KK})$, while the natural scale for mass terms localized on the $y = 0$ brane should be $\sim M_{KK} \exp(kR\pi)$, which is exponentially larger [20,33]. In our construction, then, naturalness suggests that we localize the higher-scale physics (the SM, with a scale of roughly $O(250 \text{ GeV})$) on the $y = 0$ brane, and the lower-scale DM sector with a scale of $O(0.1 - 1 \text{ GeV})$ localized on the $y = \pi R$ brane. Furthermore, the hierarchy between the two scales roughly sets the value of the product kR , namely, we must require that $e^{-kR\pi} \sim O(0.1 - 1 \text{ GeV})/O(250 \text{ GeV})$. Thus we will require that $kR \approx 1.5 - 2$. We

note in passing, therefore, that in contrast to the flat space model, the warped space construction offers the aesthetically appealing characteristic of explaining the mild hierarchy between the brane-localized vev of the SM Higgs and the brane-localized mass parameters of the DM and DP fields appearing on the opposite brane.

With these concerns addressed, we can now move on to determining the bulk profiles and sums of KK modes required for our analysis. First, we note that the equations of motion for the bulk profile $v_n(y)$ become⁴

$$\begin{aligned} \partial_y[e^{-2ky} \partial_y v_n(y)] &= -m_n^2 v_n(y), \\ (\partial_y + m_n^2 \tau R)v_n(y)|_{y=0} &= 0, \\ (e^{-2kR\pi} \partial_y + m_n^2 R)v_n(\pi R)|_{y=\pi R} &= 0.1 \end{aligned} \quad (33)$$

The solution to these equations can be written,

$$\begin{aligned} v_n(y) &= A_n z_n^W \zeta_1^{(n)}(z_n^W), \\ z_n^W &\equiv x_n^W e^{k(y-\pi R)}, \quad x_n^W \equiv \frac{m_n}{M_{KK}}, \quad \varepsilon_n^W \equiv x_n^W e^{-kR\pi} \end{aligned} \quad (34)$$

where A_n is a normalization factor, and the function $\zeta_\nu^{(n)}(z)$ is given by

$$\begin{aligned} \zeta_\nu^{(n)}(z) &\equiv \alpha_n J_\nu(z) - \beta_n Y_\nu(z), \\ \alpha_n &\equiv [(Y_0(\varepsilon_n^W) + (\varepsilon_n^W)kR\tau Y_1(\varepsilon_n^W))], \\ \beta_n &\equiv [(J_0(\varepsilon_n^W) + (\varepsilon_n^W)kR\tau J_1(\varepsilon_n^W))], \end{aligned} \quad (35)$$

with J_ν, Y_ν denoting order- ν Bessel functions of the first and second kind, respectively. Notice that $v_n(y)$ then automatically satisfies its boundary condition at the brane $y = 0$, while the allowed values of x_n^W (and hence the masses of the KK tower modes m_n) are then found with the boundary condition at $y = \pi R$, which can be simplified to

$$\begin{aligned} x_n^W \zeta_0^{(n)}(x_n^W) &= -a_W^2 \zeta_1^{(n)}(x_n^W), \\ a_W &\equiv \sqrt{kR} \frac{m_n}{M_{KK}}. \end{aligned} \quad (36)$$

The normalization constant A_n can be found using the orthonormality relation of Eq.(8), yielding

$$A_n = \frac{\sqrt{2kR}}{\left[(z_n^W)^2 [\zeta_1^{(n)}(z_n^W)^2 - \zeta_0^{(n)}(z_n^W)\zeta_2^{(n)}(z_n^W)]|_{z_n^W=\varepsilon_n^W}^{z_n^W=x_n^W} + 2\tau kR (\varepsilon_n^W)^2 \zeta_1^{(n)}(\varepsilon_n^W)^2 \right]^{1/2}}. \quad (37)$$

Using Eqs.(34) and (36), we can now continue on to an exploration of the phenomenology of various KK modes, much as we have done in Section 3 for the scenario with a flat extra dimension. We begin, as in the case of flat space, by determining the dependencies of the lowest-lying root of Eq.(36), x_1^W , as a function of the parameters (τ, a_W) , depicted in Fig. 10. Note that in Fig. 10 and subsequent calculations, we have elected to specify the parameter $(kR)\tau$ (that is τ scaled by the quantity kR) rather than τ . This is because in practice, expressions featuring the brane term τ in this setup will always do so through the quantity $(kR)\tau$; we therefore find, as has been the case in other work with RS brane terms [16], that $(kR)\tau$ is the more natural parameter to use.

Qualitatively, we observe largely similar behavior for the root x_1^W in Fig. 10 as we observed in x_1^F in Fig. 1, namely that $x_1^W \lesssim 1$ for the range of (τ, a_W) parameters we probe, and that x_1^W increases with increasing a_W and decreases with increasing τ . It is interesting to note that the specific values of x_1^W are somewhat sensitive to the specific value of kR : In particular, when $kR = 2.0$, the values of x_1^F for a given

⁴Here we use the label ‘‘W’’ to denote the values relevant for the warped scenario.

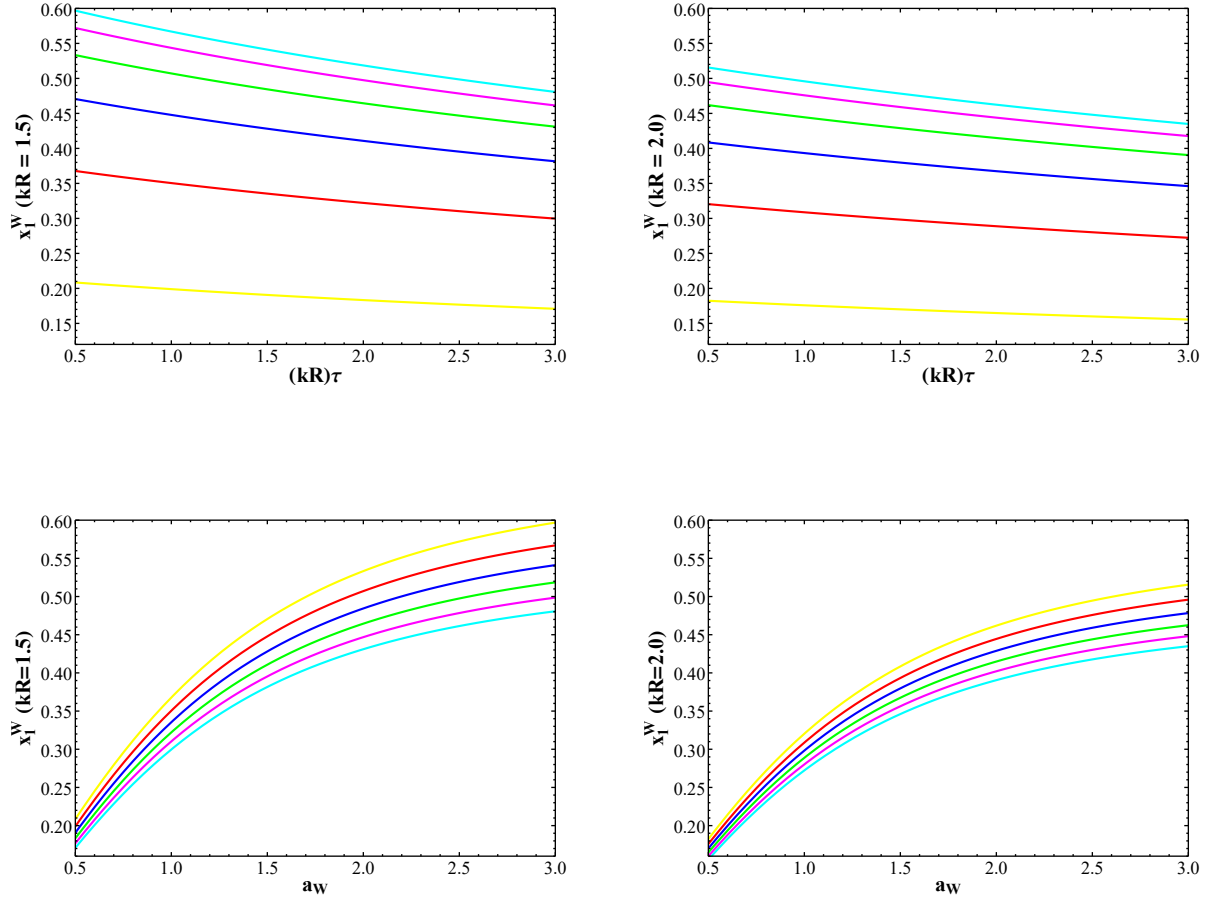


Figure 10: (Top Left) Value of the root x_1^W assuming $kR = 1.5$ as a function of τ for various choices of a_W , from bottom to top, $a_W = 1/2, 1, 3/2, 2, 5/2$ and 3 , respectively. (Top Right) The same as the top left, but assuming $kR = 2.0$ (Bottom Left) Value of the root x_1^W assuming as a function of a_W for various choices of τ , from top to bottom, $(kR)\tau = 1/2, 1, 3/2, 2, 5/2$ and 3 , respectively. (Bottom Right) The same as the bottom left, but assuming $kR = 2.0$

choice of $(kR)\tau$ and a_W is approximately 15% lower than these values in a scenario where $kR = 1.5$.

Next, we discuss the quantity m_2/m_1 , the ratio of the mass of the second KK mode of the dark photon field to that of the first KK mode; as in our discussion of this ratio in the flat space scenario, this quantity continues to possess substantial phenomenological importance due to the potential of the second KK mode to be an experimental signal for the existence of extra dimensions. In Fig. 11, we depict this mass ratio's dependence on the quantities τ and a_W . The most salient difference between the results here and those for the flat space case discussed in Section 3 lies in the typical magnitude of the ratio itself: With a flat extra dimension, we found that reasonable selections for τ and a_F resulted in ratios $m_2/m_1 \sim 3 - 4$. In the warped setup, we find that the same ratio now typically lies within the range of $m_2/m_1 \sim 6 - 16$. This represents one of the primary distinctions between the warped and flat constructions, namely, that for a given mass of the lightest KK mode of the dark photon, m_1 , *the mass of the second KK mode m_2 is significantly greater in the case of a warped extra dimension than it is in the case of a flat one.* Beyond this observation, we also note that changing kR in our computations below has an effect roughly in line with what we might expect from the results depicted in Fig. 1, namely, that a larger value of kR slightly increases the ratio m_2/m_1 , likely because the value of the root x_1^W is somewhat reduced.

We complete our exploration of the relative masses of various KK modes just as we have in the flat space scenario, namely, by exploring the growth of m_n as n increases. We depict the results in Fig. 12 for both $kR = 1.5$ and $kR = 2.0$, for various selections of $(kR)\tau$ and a_W . The most salient contrast between these results and those in the flat space analysis again lies in the magnitude of the mass ratio: In the warped setup, m_n/m_1 increases significantly more sharply with n than it does in the flat space, such that at large n , typical values of m_n/m_1 are approximately three times larger for a warped extra dimension than they are for a flat one. The dominant share of this discrepancy is determinable from the mass eigenvalue equation Eq.(36)– numerically, it can be readily seen that the difference between successive roots of this equation approaches π as n becomes large, so the eventual slope of the line depicted in Fig. 12 should be roughly $\pi(x_1^W)^{-1}$. This is compared to the analogous slope in the flat space scenario, which, as discussed in Section 3, should be approximated by $(x_1^F)^{-1}$. Because the typical values of x_1^F and x_1^W are roughly comparable, this in turn suggests that the slope of the lines in Fig. 12 should be steeper by roughly a factor of $O(\pi)$ than their flat space counterparts in Fig. 3. Before moving on, we also note that the same behavior with increasing kR that we observed in the ratio m_2/m_1 appears again as we consider more massive KK modes, namely, that increasing kR will increase the value of the ratios of heavier KK mode masses to that of the lightest mode.

Having addressed the masses of the various dark photon KK modes, we now move on to discuss the effective kinetic mixing and DM coupling terms that arise in this construction. In Fig. 13, we depict the behavior of the ratios ϵ_n/ϵ_1 and $|g_{DM}^n/g_D|$ as a function of the KK mode n (we note that once again, as in the flat space scenario, the values of g_{DM}^n oscillate in sign). The results are qualitatively quite similar to the flat space scenario depicted in Fig. 5. In particular, we find once again that while ϵ_n/ϵ_1 consistently decreases for large n , $|g_{DM}^n/g_D|$ again approaches a non-zero asymptotic value. This asymptotic value for $|g_{DM}^n/g_D|$, much like its flat space analogue, can be explored further by semi-analytical means. By using Eqs.(34) and (36), as well as the identities,

$$\begin{aligned} J_1(z)Y_0(z) - J_0(z)Y_1(z) &= \frac{2}{\pi z}, \\ \zeta_2^{(n)}(z) &= \frac{2}{z}\zeta_1^{(n)}(z) - \zeta_0^{(n)}(z), \end{aligned} \quad (38)$$

it is possible to determine that as n becomes very large, the ratio $|g_{DM}^n/g_D|$ becomes well-approximated by the expression

$$\begin{aligned} \left| \frac{g_{DM}^n}{g_D} \right| &\approx \frac{1}{(x_1^W)} \left((x_1^W)^2 + 2a_W^2 + a_W^4 - (1 + (kR)^2\tau^2(x_1^W)^2 e^{-2kR\pi}) \left(\mathcal{J} \right)^2 \right)^{\frac{1}{2}}, \\ \mathcal{J} &\equiv \frac{x_1^W J_0(x_1^W) + a_W^2 J_1(x_1^W)}{J_0(x_1^W e^{-kR\pi}) + (kR)\tau x_1^W e^{-kR\pi} J_1(x_1^W e^{-kR\pi})}. \end{aligned} \quad (39)$$

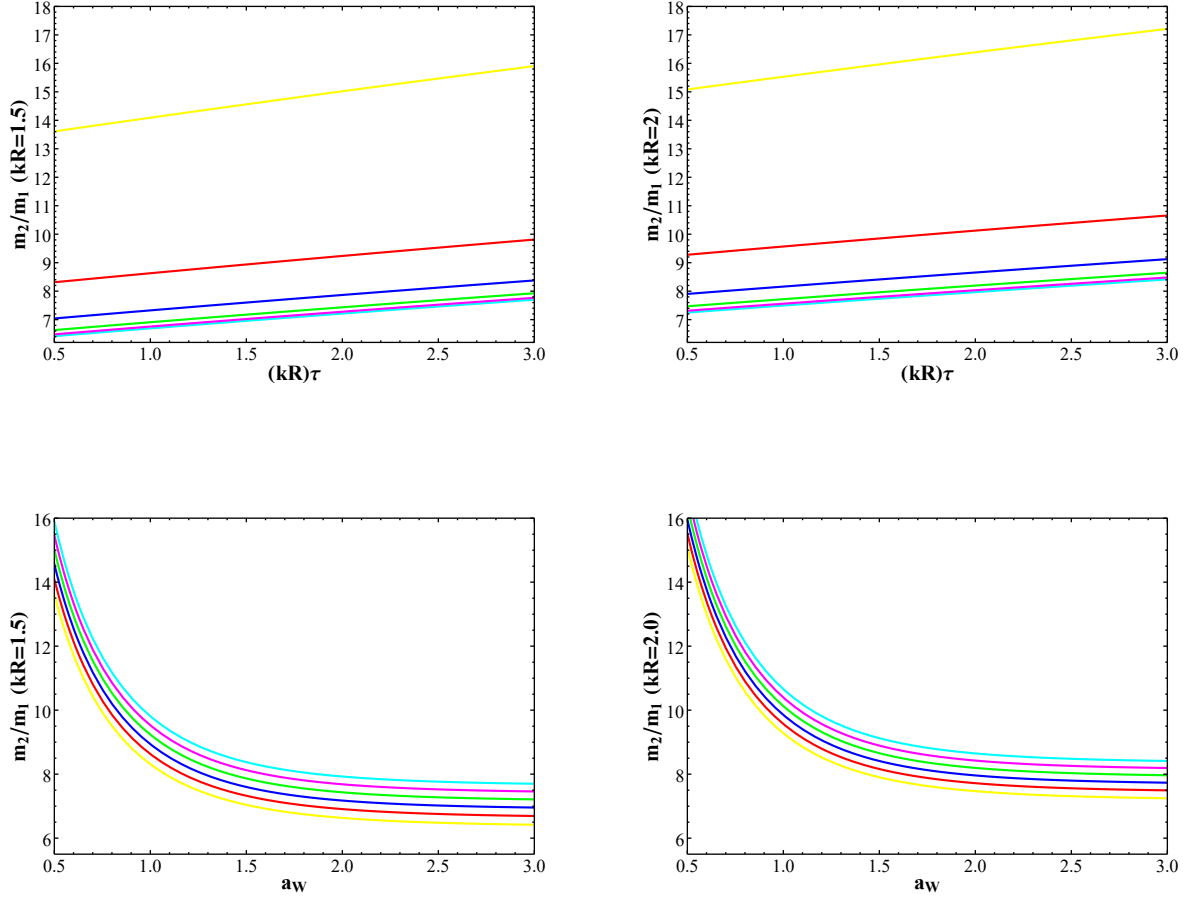


Figure 11: (Top Left) The mass ratio of the lowest two DP KK states, $m_2/m_1 = x_2^W/x_1^W$ assuming $kR = 1.5$, as a function of $(kR)\tau$ for $a_W = 3$ (cyan), $5/2$ (magenta), 2 (green), $3/2$ (blue), 1 (red), and $1/2$ (yellow), respectively. (Top Right) As in the top left, but now assuming $kR = 2.0$. (Bottom Left) As in the top left, but now as a function of a_W assuming $(kR)\tau = 3$ (cyan), $5/2$ (magenta), 2 (green), $3/2$ (blue), 1 (red), and $1/2$ (yellow), respectively. (Bottom Right) As in the bottom left, but assuming $kR = 2.0$.

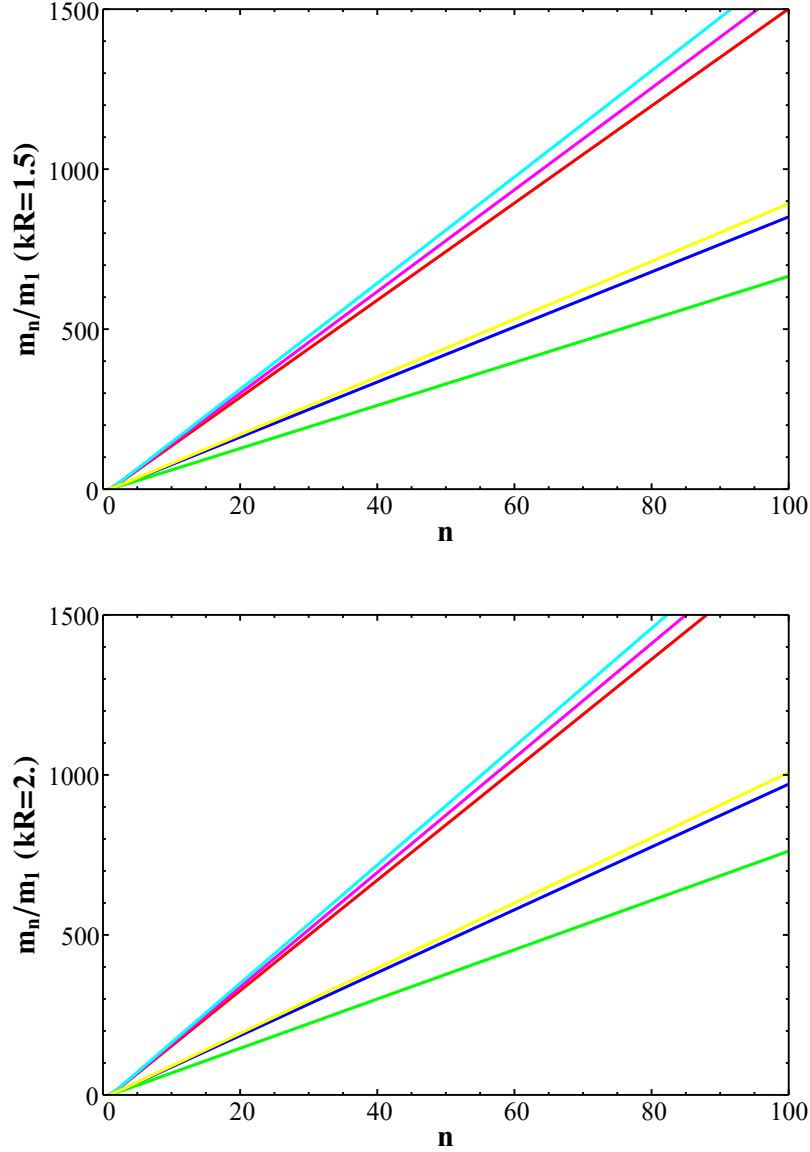


Figure 12: (Top) Approximate linear growth of the relative DP KK mass ratio m_n/m_1 as a function of n assuming $kR = 1.5$ for various choices of $((kR)\tau, a_W) = (1/2, 1/2)$ [red], $(1/2, 1)$ [blue], $(1/2, 3/2)$ [green], $(1, 1/2)$ [magenta], $(3/2, 1/2)$ [cyan] and $(1, 1)$ [yellow], respectively. (Bottom) As in the previous panel, but assuming $kR = 2.0$

In Fig. 14, we depict the dependence of this approximate asymptotic value on τ and a_W . The behavior of this quantity is quite similar to the analogous results Fig. 4 for the flat space scenario, in particular, we observe a sharp increase in the ratio here as a_W increases, just as the corresponding ratio in the flat space case increases sharply with increasing a_F . We note that the typical maximum values that we observe in Fig. 14, however, are roughly a factor of 2 smaller than those we observed in Fig. 4, however, as a_F and a_W are not directly comparable quantities, the significance of this diminished range is not obvious. Again, as in Fig. 4, we have included a dashed line which denotes the maximum value that this ratio can attain such that all g_{DM}^n remain perturbative for the choice $g_D = 0.3$; in this case, we see that such a requirement effectively excludes choices of $a_W \gtrsim 2$.

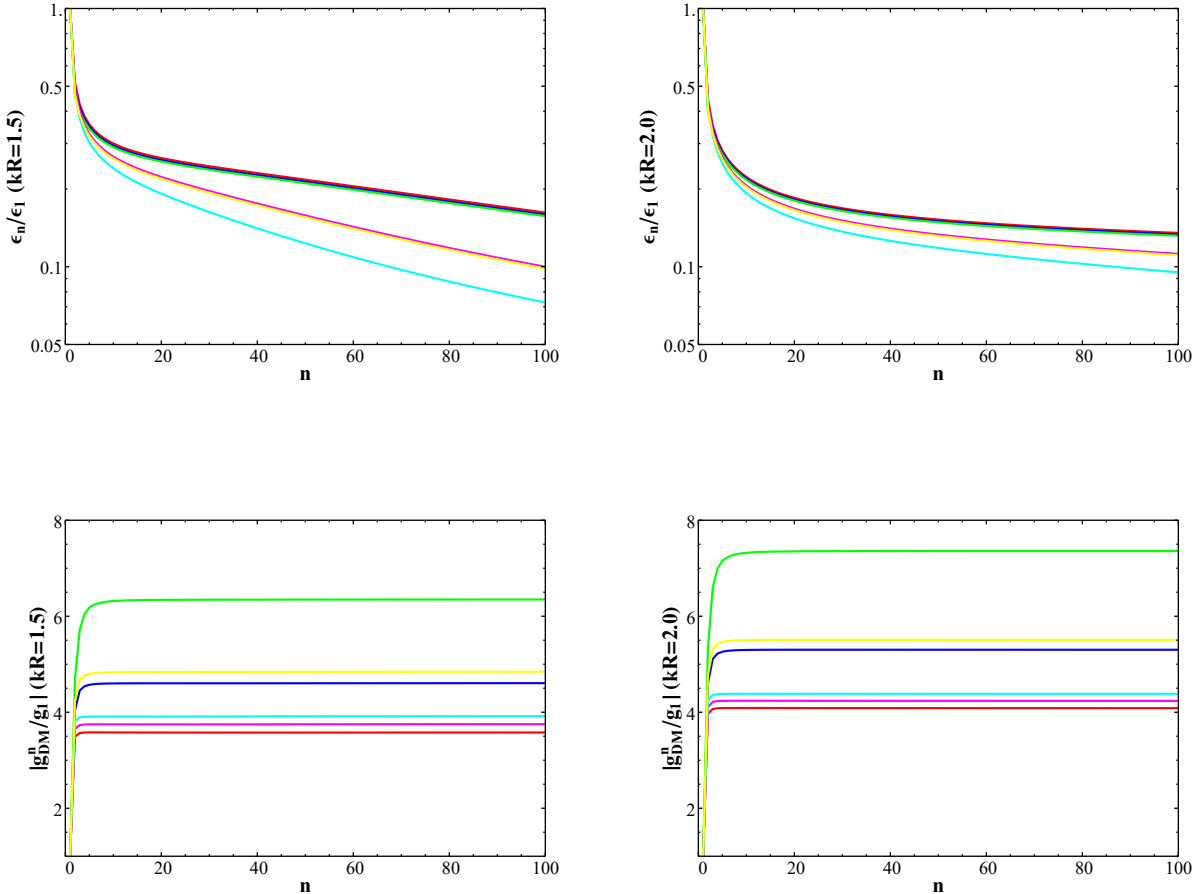


Figure 13: (Top Left) The ratio ϵ_n/ϵ_1 , assuming $kR = 1.5$, as a function of n for various choices of $((kR)\tau, a_W) = (1/2, 1/2)$ [red], $(1/2, 1)$ [blue], $(1/2, 3/2)$ [green], $(1, 1/2)$ [magenta], $(3/2, 1/2)$ [cyan] and $(1, 1)$ [yellow], respectively. (Top Right) The same as the top left, but assuming $kR = 2.0$ (Bottom Left) The ratio g_{DM}^n/g_D , assuming $kR = 1.5$, as a function of n for various choices of $((kR)\tau, a_W) = (1/2, 1/2)$ [red], $(1/2, 1)$ [blue], $(1/2, 3/2)$ [green], $(1, 1/2)$ [magenta], $(3/2, 1/2)$ [cyan] and $(1, 1)$ [yellow], respectively. (Bottom Right) The same as the bottom left, but assuming $kR = 2.0$

Just as in our analysis of the flat space setup, we can now move on from discussing individual KK modes' masses and couplings to the basic predictions of phenomenologically important processes. In order to do this, we must first evaluate the sum $F(y, y', s)$ (defined in Eq.(9) for the warped metric, by

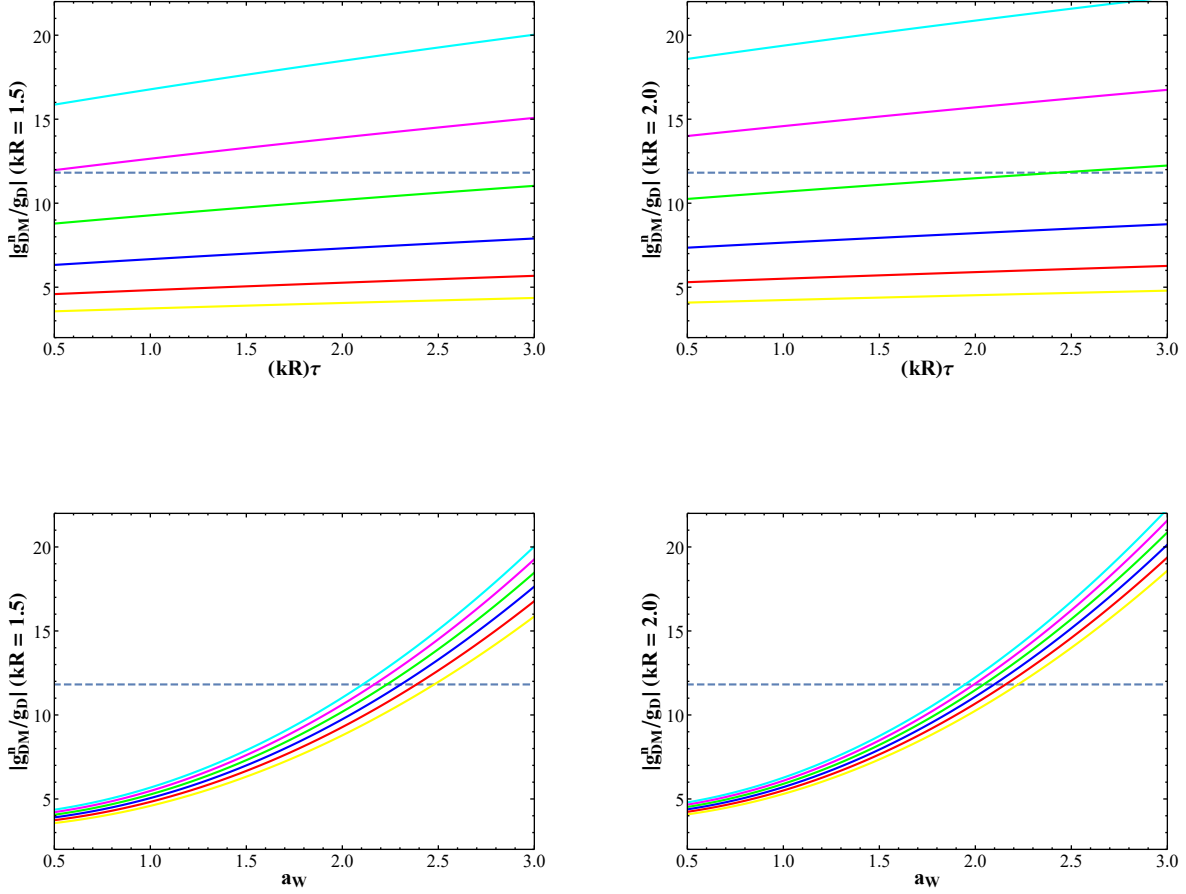


Figure 14: (Top Left) The approximate asymptotic value of $|g_{DM}^n/g_D|$ given by Eq.(39) for large n , assuming $kR = 1.5$, as a function of $(kR)\tau$ for various choices of $a_W = 3$ (cyan), $5/2$ (magenta), 2 (green), $3/2$ (blue), 1 (red), $1/2$ (yellow). (Top Right) The same as the top left, but assuming $kR = 2.0$ (Bottom Left) The approximate asymptotic value of $|g_{DM}^n/g_D|$ given by Eq.(39) for large n , assuming $kR = 2.0$, as a function of a_W for various choices of $(kR)\tau = 3$ (cyan), $5/2$ (magenta), 2 (green), $3/2$ (blue), 1 (red), $1/2$ (yellow). The dashed line represents the maximum value that this ratio can obtain and still have all KK couplings remain perturbative for $g_D = 0.3$. (Bottom Right) The same as the bottom left, but assuming $kR = 2.0$

solving Eq.(13) with $f(y) = e^{-ky}$ inserted. We arrive at the differential equation

$$\partial_y [e^{-2ky} \partial_y F(y, y', s)] = R\delta(y - y') - sF(y, y', s), \quad (40)$$

$$\partial_y F(y, y', s)|_{y=0} = -s\tau R F(0, y', s), \quad (41)$$

$$\partial_y F(y, y', s)|_{y=\pi R} = -m_V^2 R e^{-2kR\pi} F(\pi R, y', s). \quad (42)$$

By defining the variables $z \equiv (\sqrt{s}/M_{KK})e^{k(y-\pi R)}$ and $z' \equiv (\sqrt{s}/M_{KK})e^{k(y'-\pi R)}$, we can solve Eq.(40) in terms of Bessel functions, yielding

$$F(y, y', s) = -\frac{kR\pi}{2M_{KK}^2} \frac{e^{k(y+y'-2\pi R)} \xi_1(z_>) \omega_1(z_<)}{z_\pi \omega_0(z_\pi) + a_W^2 \omega_1(z_\pi)}, \quad (43)$$

$$\omega_\nu(z) \equiv [Y_0(z_0) + \tau k R z_0 Y_1(z_0)] J_\nu(z) - [J_0(z_0) + \tau k R z_0 J_1(z_0)] Y_\nu(z),$$

$$\xi_\nu(z) \equiv [z_\pi Y_0(z_\pi) + a_W^2 Y_1(z_\pi)] J_\nu(z) - [z_\pi J_0(z_\pi) + a_W^2 J_1(z_\pi)] Y_\nu(z),$$

$$z_> \equiv \left(\frac{\sqrt{s}}{M_{KK}}\right) e^{k(\max(y, y') - \pi R)}, \quad z_< \equiv \left(\frac{\sqrt{s}}{M_{KK}}\right) e^{k(\min(y, y') - \pi R)},$$

$$z_0 \equiv \left(\frac{\sqrt{s}}{M_{KK}}\right) e^{-kR\pi}, \quad z_\pi \equiv \left(\frac{\sqrt{s}}{M_{KK}}\right).$$

We note that in this form, it is readily apparent that $F(y, y', s)$ has poles wherever \sqrt{s} is equal to the mass of a KK mode m_n , just as we would expect given the components of its sum and just as we previously observed in the flat-space sum Eq.(27).

With a solution for $F(y, y', s)$ in hand, we can then replicate our analysis in Section 3 to determine whether or not our kinetic mixing treatment is valid in the parameter space we're probing, this time applied to the warped space scenario not considered in I. Through analogous steps to those taken in Section 3, we find that the sum $\sum_n \epsilon_n^2/\epsilon_1^2$ in the case of warped spacetime is also given by

$$\sum_n \epsilon_n^2/\epsilon_1^2 = \frac{1}{\tau v_1(0)^2}, \quad (44)$$

the only difference from the flat-space result here being the form of the function $v_1(0)$. The τ^{-1} dependence of this sum suggests the same requirements as the identical flat space result, then: The BLKT τ must still be large enough so that its magnitude remains $\lesssim 10$ and positive so that the result does not require the existence of ghost states. In Fig. 15, we depict the sum $\sum_n \epsilon_n^2/\epsilon_1^2$ for different values of τ and a_W . Notably, while the sum is generally within reasonable $\lesssim 10$ limits, when $(kR)\tau \approx 1/2$, the sum becomes quite close to, and even somewhat exceeds, 10. While the largest values of $\sum_n \epsilon_n^2/\epsilon_1^2$ achieved among the region of parameter space we have explored still aren't quite large enough to render ϵ_1^2 terms in our analysis numerically significant (at least for the $\epsilon_1 \sim 10^{-(3-4)}$ terms we consider here), the sharp rate of increase they enjoy with decreasing τ near $(kR)\tau = 1/2$ suggests that probing significantly below this value is unlikely to yield valid results. On the surface, this may seem to contrast slightly with our results in Section 3, in which we found that restricting τ to values larger than 1/2 stayed roughly $\lesssim 6$. Closer inspection indicates that this discrepancy can largely be attributed to the use of $(kR)\tau$ as the variable we are employing instead of τ : If one compares the maximum value obtained by the warped sum at $(kR)\tau = 3/4$ (for $kR = 1.5$) and $(kR)\tau = 1$ (for $kR = 2.0$), for which the variable τ itself is simply 1/2, the results for the sum with both kR values very closely matches that which was observed in the flat space construction of Section 3. Hence, in both the flat and warped space cases, our setup's treatment of kinetic mixing easily remains valid for $\tau \gtrsim 0.5$, although it should be noted that as kR increases, any boundary from these perturbativity concerns on the more natural warped-space parameter $(kR)\tau$, which is often used instead of τ for warped setups [16], will become increasingly stringent.

Moving on, it is then straightforward to find the DM- e^- scattering cross section by inserting our

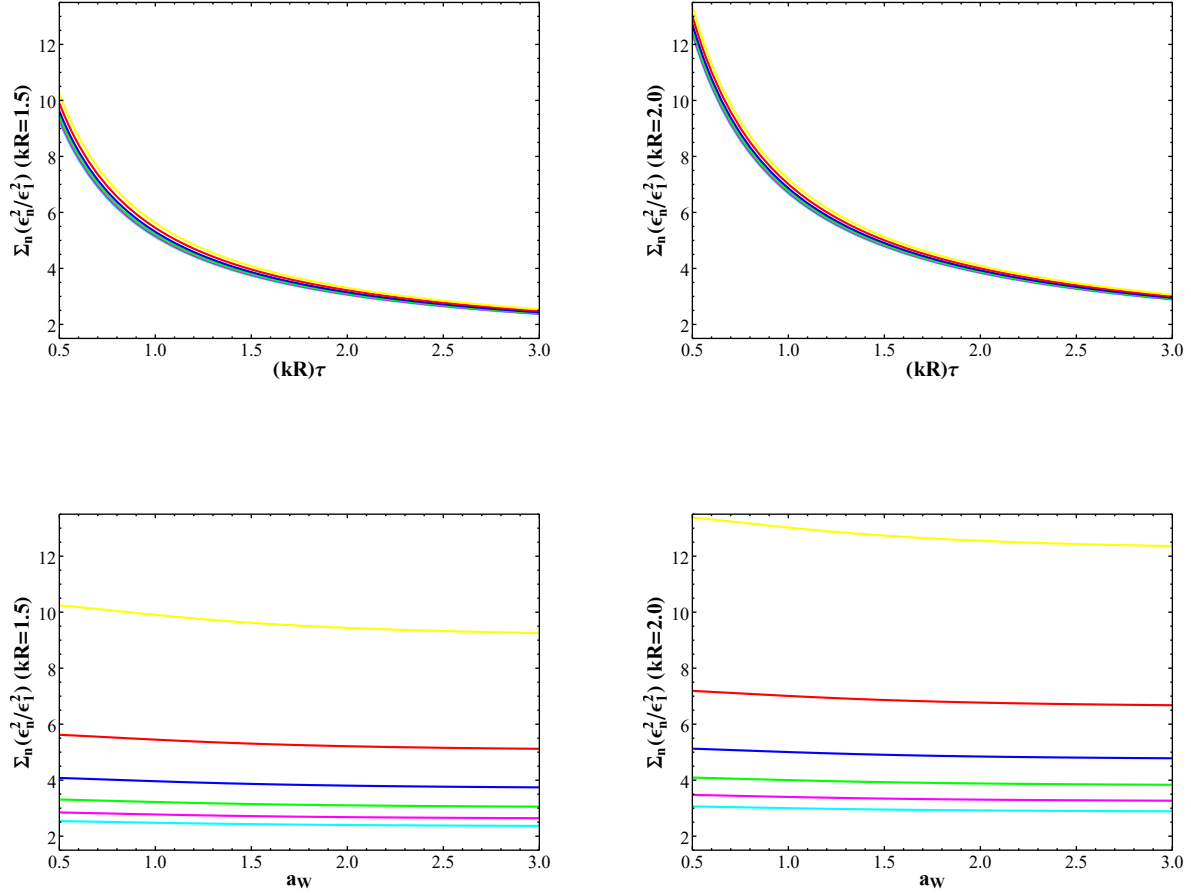


Figure 15: (Top Left) The value of the sum $\sum_n \epsilon_n^2/\epsilon_1^2$ over all n assuming $kR = 1.5$, as a function of $(kR)\tau$ for $a_W = 3$ (cyan), $5/2$ (magenta), 2 (green), $3/2$ (blue), 1 (red), and $1/2$ (yellow), respectively. (Top Right) As in the top left, but now assuming $kR = 2.0$. (Bottom Left) As in the top left, but now as a function of a_W assuming $(kR)\tau = 3$ (cyan), $5/2$ (magenta), 2 (green), $3/2$ (blue), 1 (red), and $1/2$ (yellow), respectively. (Bottom Right) As in the bottom left, but assuming $kR = 2.0$.

results for $F(y, y', s)$ given in Eq.(43) into Eq.(15), arriving at

$$\sigma_{\phi e} = \frac{4\alpha_{\text{em}}m_e^2(g_D\epsilon_1)^2}{v_1(\pi R)^2v_1(0)^2} \frac{(kR)^2}{a_W^4 M_{KK}^4} = (2.97 \times 10^{-40} \text{ cm}^2) \left(\frac{100 \text{ MeV}}{m_1}\right)^4 \left(\frac{g_D\epsilon_1}{10^{-4}}\right)^2 \Sigma_{\phi e}^W, \quad (45)$$

$$\Sigma_{\phi e}^W \equiv \frac{(x_1^W)^4(kR)^2}{a_W^4 v_1(\pi R)^2 v_1(0)^2} = \left| \sum_{n=0}^{\infty} \frac{(x_1^F)^2 v_n(0) v_n(\pi R)}{(x_n^F)^2 v_1(0) v_1(\pi R)} \right|^2. \quad (46)$$

Notably, this is the same result (up to a normalization convention of the parameter a_W and, of course, different bulk wave functions $v_1(y)$) that we derived for the flat-space case Eq.(30). In particular, the sum $F(0, \pi R, 0)$ has *identical* results (again, up to normalization of a_W) for the flat- and warped-space scenarios. Just as in the flat space case, the numerical coefficient in front of the quantity $\Sigma_{\phi e}^W$, which now encapsulates all of the cross section's dependence on the parameters τ and a_W , indicates that as long as $\Sigma_{\phi e}^W \lesssim 1$, the resultant cross section is not constrained by current experimental limits, although we remind the reader that such cross sections may lie within reach of near-term future direct-detection experiments. In Fig. 16, we depict the dependence of $\Sigma_{\phi e}^W$ on various choices of τ and a_W ; we find that just as for the flat space case, this requirement is easily satisfied for every τ and a_W we consider.

We also note that the sum over individual KK modes in the computation of $\Sigma_{\phi e}^W$ quickly converges to the closed form expression even when truncated for very low n ; as depicted in Fig. 17, $\Sigma_{\phi e}^W$, just like its flat space analogue, converges to within $O(10^{-2})$ corrections to its exact value even when truncated at $n \approx 10$. Hence, just as in the flat space scenario, exchanges of the lightest few DP KK modes dominate the direct detection signal.

Finally, we can conclude our discussion of the warped space scenario by considering the thermally averaged annihilation cross section of DM particles into SM fermions. Inserting the relevant value of $F(y, y', s)$ into Eq.(19) allows us to derive the DM annihilation cross-section, σv_{lab} , for the warped space scenario, yielding

$$\begin{aligned} \sigma v_{lab} = & \frac{1}{3} \frac{g_D^2 \epsilon_1^2 \alpha_{\text{em}} Q_f^2}{v_1(\pi R)^2 v_1(0)^2} \frac{(s + 2m_f^2)(s - 4m_{DM}^2) \sqrt{s(s - 4m_f^2)}}{s(s - 2m_{DM}^2) M_{KK}^4} \\ & \times \left| \frac{2}{\pi z_\pi} \left(\frac{kR}{z_\pi \omega_0(z_\pi) + a_W^2 \omega_1(z_\pi)} \right) - \frac{v_1(\pi R) v_1(0)}{(s/M_{KK}^2) - (x_1^W)^2} + \frac{v_1(\pi R) v_1(0)}{(s/M_{KK}^2) - (x_1^W)^2 + ix_1^W \Gamma_1/M_{KK}} \right|^2, \end{aligned} \quad (47)$$

where we remind the reader that the functions $\omega_{0,1}(z)$ are defined in Eq.(43). Inserting this result into Eq.(16), we can straightforwardly obtain the thermally averaged DM annihilation cross section via numerical integration. Just as in the flat space case, we specify that $m_{DM} = 100 \text{ MeV}$, $x_F = (m_{DM}/T) = 20$, $g_D = 0.3$, and $g_D\epsilon_1 = 10^{-4}$, and consider DM annihilation into an e^+e^- final state. Our results, depicted in Fig. 18 along with a dashed line marking $\langle \sigma v \rangle = 7.5 \times 10^{-26} \text{ cm}^3/\text{s}$, the approximate necessary cross section to produce the observed DM relic abundance, exhibit substantial similarity with the results for the flat space scenario given in Fig. 9; in particular, in both cases the dependence of the cross section on the BLKT τ and the brane-localized mass parameter $m_V \propto a_{F,W}$ is extremely limited, and the correct relic abundance is obtained when $m_{DM} \approx 0.36m_1$ or $m_{DM} \approx 0.53m_1$. Of course, as we vary the DM mass and $g_D\epsilon_1$, other values of m_1 will also be allowed. In short, for the annihilation cross section at freeze-out, we observe qualitatively similar behavior in the warped space setup as we do in the flat space scenario: For our choice of parameters resonant enhancement is necessary in order to realize the correct dark matter relic density, and the cross section is largely agnostic to specific selections for the brane-localized kinetic and mass terms for the DP field.

5 Summary and Conclusions

In this paper, we have discussed a modification to our previous setup in I and II. In lieu of imparting mass to the lightest dark photon KK modes via dark photon boundary conditions, which necessitates a bulk DM particle with corresponding KK modes, our current construction simplifies this structure

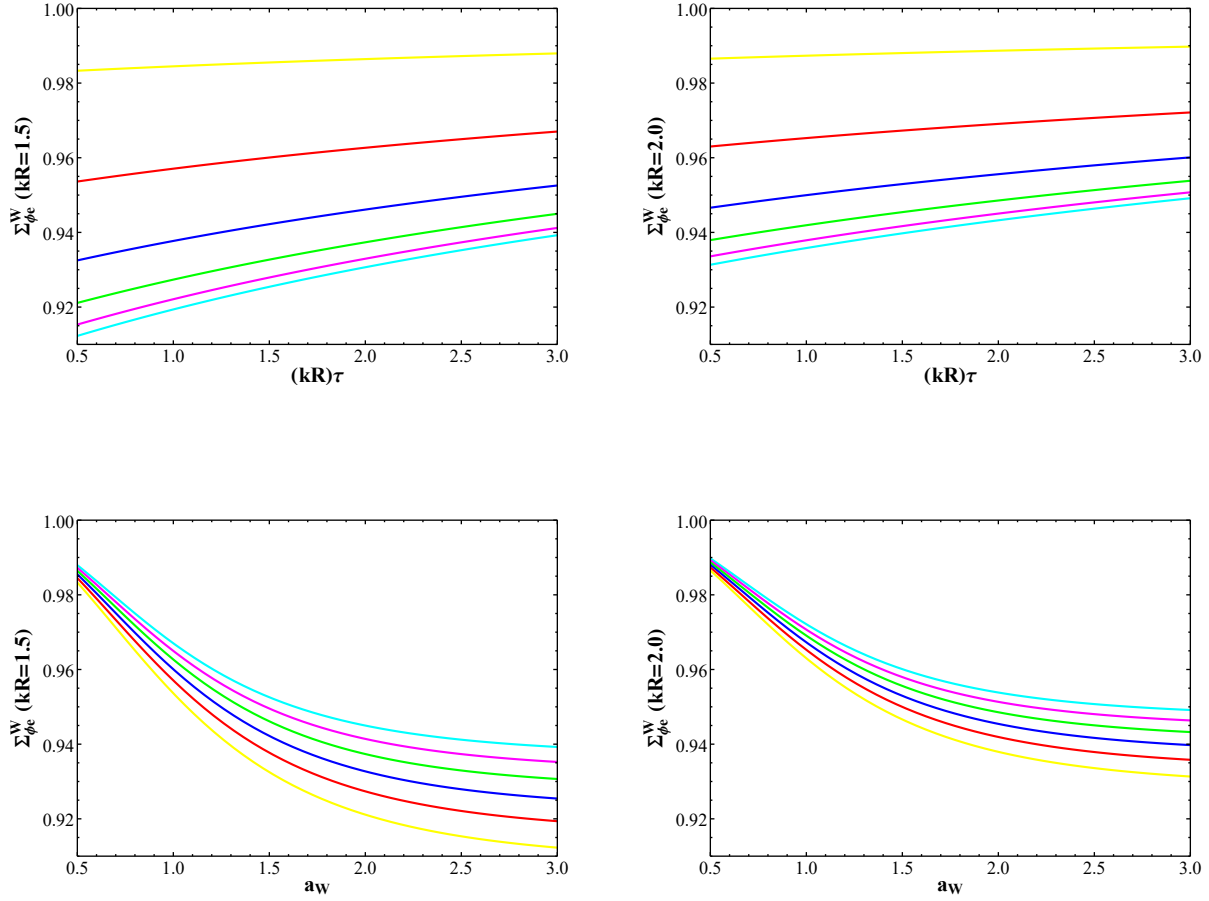


Figure 16: (Top Left) The sum $\Sigma_{\phi_e}^W$ defined in Eq.(45), assuming $kR = 1.5$, as a function of $(kR)\tau$ for $a_W = 3$ (cyan), $5/2$ (magenta), 2 (green), $3/2$ (blue), 1 (red), and $1/2$ (yellow), respectively. (Top Right) As in the top left, but now assuming $kR = 2.0$. (Bottom Left) As in the top left, but now as a function of a_W assuming $(kR)\tau = 3$ (cyan), $5/2$ (magenta), 2 (green), $3/2$ (blue), 1 (red), and $1/2$ (yellow), respectively. (Bottom Right) As in the bottom left, but assuming $kR = 2.0$.

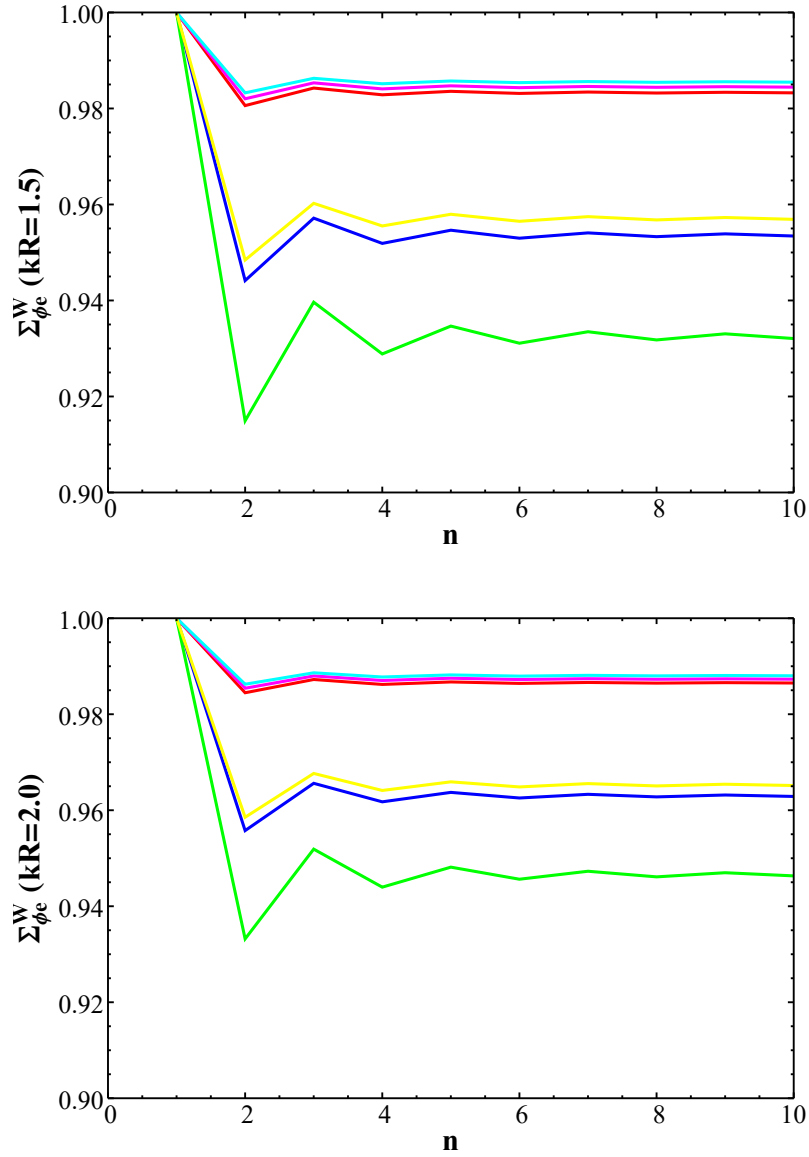


Figure 17: (Top) The value of the sum $\Sigma_{\phi_e}^W$ defined in Eq.(45) truncated at finite n , assuming $kR = 1.5$ for various choices of $((kR)\tau, a_W) = (1/2, 1/2)$ [red], $(1/2, 1)$ [blue], $(1/2, 3/2)$ [green], $(1, 1/2)$ [magenta], $(3/2, 1/2)$ [cyan] and $(1, 1)$ [yellow], respectively. (Bottom) As in the previous panel, but assuming $kR = 2.0$

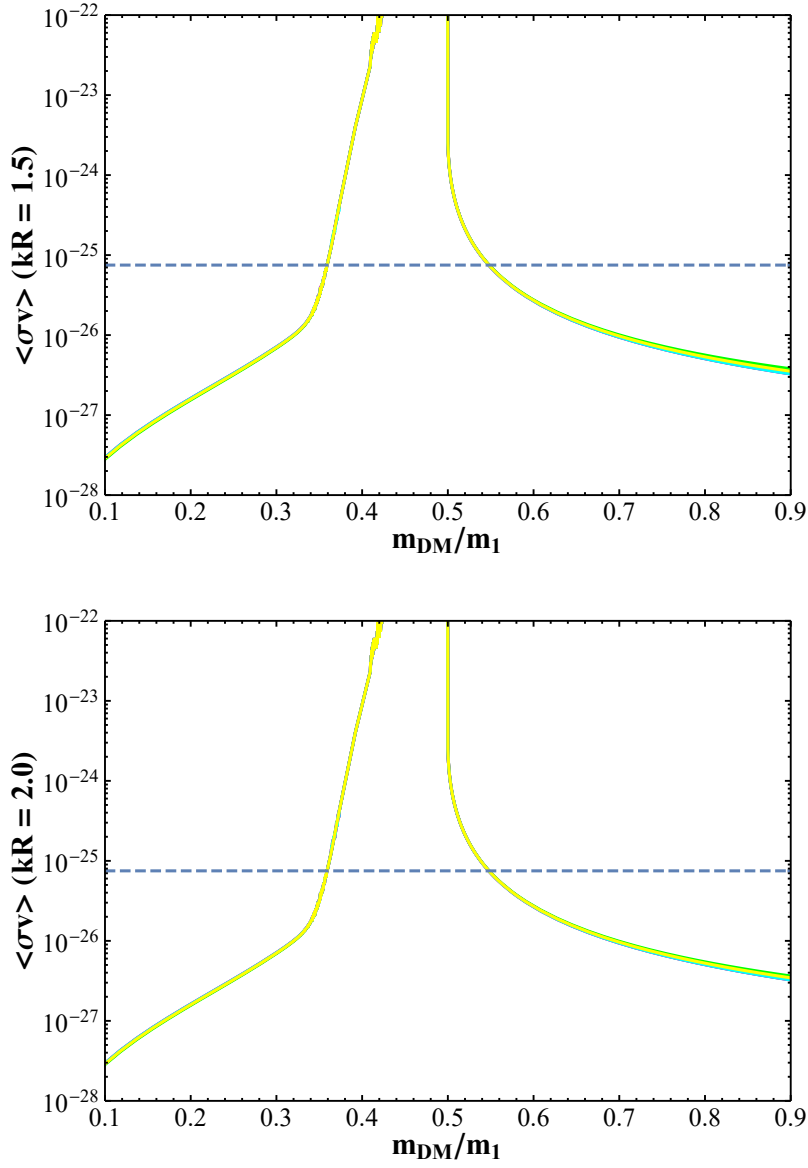


Figure 18: (Top) The thermally averaged annihilation cross section in cm^3/s , assuming $kR = 1.5$ for various choices of $((kR)\tau, a_W) = (1/2, 1/2)$ [red], $(1/2, 1)$ [blue], $(1/2, 3/2)$ [green], $(1, 1/2)$ [magenta], $(3/2, 1/2)$ [cyan] and $(1, 1)$ [yellow], respectively. (Bottom) As in the previous panel, but assuming $kR = 2.0$

by reinstating the dark Higgs as a scalar localized on the *opposite* brane in the theory from the brane containing the SM, preventing mixing between the SM and dark Higgs scalars. The DM particle can then be placed on the same brane as the dark Higgs, removing the additional complication of a KK tower of DM particles and resulting in substantially simpler phenomenology while still removing the effects of the dark and SM Higgses mixing.

We then briefly explored the model-building possibilities for this setup in two scenarios, one with a flat extra dimension and the other with a warped RS metric, in particular considering the behavior of the DP tower's mass spectrum, couplings, and mixing parameters with SM fields, as well as briefly touching on the predictions for SI direct detection experiments and thermally averaged annihilation cross sections at freeze-out for various points in parameter space. Exploring the case of a warped extra dimension in addition to that of a flat one affords us significant additional model-building freedom; for example, given the same choice for the lightest DP KK mode mass, subsequent KK modes for the warped scenario are approximately ~ 3 times heavier than they are in the flat scenario, demonstrating a qualitatively different KK spectrum. The ability for warped extra dimensions to generate hierarchies, meanwhile, can be straightforwardly exploited to naturally explain the mild $O(10^{2-3})$ hierarchy that exists between the SM Higgs scale and the characteristic mass scales of the dark brane, namely the masses of the DM and the lightest DP KK modes $\sim 0.1 - 1$ GeV.

With this model, we find few parameter space restrictions in either the warped or flat space constructions. The requirement that every DP KK mode's coupling to DM remain perturbative provides an upper limit on the DM-brane-localized mass term m_V , in particular, we find that for the flat construction, $m_V \lesssim 1.5R^{-1}$, where R is the compactification radius of the extra dimension, while for warped space, $m_V \lesssim 2M_{KK}/\sqrt{kR}$, where M_{KK} is the KK mass in the model and $kR \sim 1.5 - 2.0$. We also find, in agreement with I for the flat space scenario and novelly for the case of warped space, that a positive $O(1)$ value for the SM-brane-localized kinetic term (referred to here as τ) is necessary in order to ensure the validity of our kinetic mixing analysis (in particular to ensure that $O(\epsilon_1^2)$ and higher order terms can in fact be safely neglected). For both the flat and warped space scenarios, however, this constraint is quite mild; requiring $\tau \geq 1/2$ is sufficient to satisfy it.

Regarding possible experimental signals, we explicitly consider that of SI direct detection from scattering with electrons. We find that selecting $g_D\epsilon_1 \sim 10^{-4}$ and $m_1 \sim 100$ MeV still places the SI direct detection cross sections in both the flat and warped space constructions at $\sim 10^{-40}\text{cm}^2$, below current experimental constraints. However, we note that such signals are roughly within the order of magnitude of the possible reach of near-term future experiments, and are not especially sensitive to variations in the brane-localized kinetic and mass terms of the particular extra dimensional model (in the flat scenario, we see reasonable variation in these parameters producing at most an approximately 25% change in the value of the DD cross section, while for the warped scenario this variation is approximately 5%). As such, experiments such as SuperCDMS may place meaningful constraints on DP KK mode masses, couplings, and mixings in the near future.

The requirement that the thermally averaged annihilation cross section for the DM gives rise to the correct DM relic density, meanwhile, substantially constrains our selection of the relative DM particle mass m_{DM}/m_1 . In particular, for natural selections of the other model parameters we see in both the flat and warped scenarios the DM annihilation cross section must enjoy some resonant enhancement of the contribution from the exchange of the lightest DP KK mode in order to attain a sufficiently large value. Given the sharpness of the resonance peak, this requirement places a significant constraint on the m_{DM} ; for the choices $g_D\epsilon_1 = 10^{-4}$, $m_1 = 100$ MeV, and $g_D = 0.3$, m_{DM} must lie near 0.36 or 0.54 of m_1 for flat space and 0.36 or 0.53 of m_1 for warped space. This cross section is also notably largely insensitive to differing choices of the brane-localized DP mass m_V and the BLKT τ provided m_1 , g_D , and ϵ_1 are kept fixed, indicating that the exchange of the lightest KK mode is, somewhat unsurprisingly given its resonant enhancement, of paramount importance as contributors to this process.

Overall, we find that constructing this model within a flat or warped space framework results in little qualitative difference in our results. The most salient potential phenomenological difference lies in the differing relative masses of DP KK modes (in particular, the ratio of the second-lightest dark photon mass to that of the lightest is in general 3-4 times larger in the RS-like metric we consider than in

the flat space case), which would have considerable effect on experimental searches for dark photons in colliders. Otherwise, however, we note that a wide range of natural and currently phenomenologically viable parameter space is available for both constructions.

As we move forward to explore the possibilities of kinetic mixing in theories of extra dimensions, we continue to find alternate constructions that allow for phenomenologically viable models. Here, following the work of I and II, we have presented another, simpler, construction that utilizes the additional model-building freedom afforded by extra dimensions to ameliorate phenomenological concerns that arise in 4D kinetic mixing theories.

Acknowledgements

The authors would like to particularly thank D. Rueter and J.L. Hewett for very valuable discussions related to this work. This work was supported by the Department of Energy, Contract DE-AC02-76SF00515.

References

- [1] For a recent review of WIMPs, see G. Arcadi, M. Dutra, P. Ghosh, M. Lindner, Y. Mambrini, M. Pierre, S. Profumo and F. S. Queiroz, arXiv:1703.07364 [hep-ph].
- [2] M. Kawasaki and K. Nakayama, *Ann. Rev. Nucl. Part. Sci.* **63**, 69 (2013) [arXiv:1301.1123 [hep-ph]].
- [3] P. W. Graham, I. G. Irastorza, S. K. Lamoreaux, A. Lindner and K. A. van Bibber, *Ann. Rev. Nucl. Part. Sci.* **65**, 485 (2015) [arXiv:1602.00039 [hep-ex]].
- [4] J. Alexander *et al.*, arXiv:1608.08632 [hep-ph].
- [5] M. Battaglieri *et al.*, arXiv:1707.04591 [hep-ph].
- [6] N. Aghanim *et al.* [Planck], [arXiv:1807.06209 [astro-ph.CO]].
- [7] There has been a huge amount of work on this subject; see, for example, D. Feldman, B. Kors and P. Nath, *Phys. Rev. D* **75**, 023503 (2007) [hep-ph/0610133]; D. Feldman, Z. Liu and P. Nath, *Phys. Rev. D* **75**, 115001 (2007) [hep-ph/0702123 [HEP-PH]].; M. Pospelov, A. Ritz and M. B. Voloshin, *Phys. Lett. B* **662**, 53 (2008) [arXiv:0711.4866 [hep-ph]]; M. Pospelov, *Phys. Rev. D* **80**, 095002 (2009) [arXiv:0811.1030 [hep-ph]]; H. Davoudiasl, H. S. Lee and W. J. Marciano, *Phys. Rev. Lett.* **109**, 031802 (2012) [arXiv:1205.2709 [hep-ph]] and *Phys. Rev. D* **85**, 115019 (2012) doi:10.1103/PhysRevD.85.115019 [arXiv:1203.2947 [hep-ph]]; R. Essig *et al.*, arXiv:1311.0029 [hep-ph]; E. Izaguirre, G. Krnjaic, P. Schuster and N. Toro, *Phys. Rev. Lett.* **115**, no. 25, 251301 (2015) [arXiv:1505.00011 [hep-ph]]; For a general overview and introduction to this framework, see D. Curtin, R. Essig, S. Gori and J. Shelton, *JHEP* **1502**, 157 (2015) [arXiv:1412.0018 [hep-ph]].
- [8] B. Holdom, *Phys. Lett.* **166B**, 196 (1986) and *Phys. Lett. B* **178**, 65 (1986); K. R. Dienes, C. F. Kolda and J. March-Russell, *Nucl. Phys. B* **492**, 104 (1997) [hep-ph/9610479]; F. Del Aguila, *Acta Phys. Polon. B* **25**, 1317 (1994) [hep-ph/9404323]; K. S. Babu, C. F. Kolda and J. March-Russell, *Phys. Rev. D* **54**, 4635 (1996) [hep-ph/9603212]; T. G. Rizzo, *Phys. Rev. D* **59**, 015020 (1998) [hep-ph/9806397].
- [9] See, for example, T. Gherghetta, J. Kersten, K. Olive and M. Pospelov, *Phys. Rev. D* **100**, no.9, 095001 (2019) doi:10.1103/PhysRevD.100.095001 [arXiv:1909.00696 [hep-ph]]; T. G. Rizzo, *Phys. Rev. D* **99**, no.11, 115024 (2019) doi:10.1103/PhysRevD.99.115024 [arXiv:1810.07531 [hep-ph]]; T. D. Rueter and T. G. Rizzo, *Phys. Rev. D* **101**, no.1, 015014 (2020) doi:10.1103/PhysRevD.101.015014 [arXiv:1909.09160 [hep-ph]]; J. H. Kim, S. D. Lane, H. S. Lee, I. M. Lewis and M. Sullivan, *Phys. Rev. D* **101**, no.3, 035041 (2020) doi:10.1103/PhysRevD.101.035041 [arXiv:1904.05893 [hep-ph]].

- [10] See, for example, I. Antoniadis, Phys. Lett. B **246**, 377 (1990); K. R. Dienes, E. Dudas and T. Gherghetta, Phys. Lett. B **436**, 55 (1998) [hep-ph/9803466] and Phys. Lett. B **436**, 55 (1998) [hep-ph/9803466]; I. Antoniadis, N. Arkani-Hamed, S. Dimopoulos and G. R. Dvali, Phys. Lett. B **436**, 257 (1998) [hep-ph/9804398]; N. Arkani-Hamed, S. Dimopoulos and G. R. Dvali, Phys. Lett. B **429**, 263 (1998) [hep-ph/9803315]; L. Randall and R. Sundrum, Phys. Rev. Lett. **83**, 3370 (1999) [hep-ph/9905221]; T. Appelquist, H. C. Cheng and B. A. Dobrescu, Phys. Rev. D **64**, 035002 (2001) [hep-ph/0012100].
- [11] T. G. Rizzo, JHEP **1807**, 118 (2018) [arXiv:1801.08525 [hep-ph]].
- [12] T. G. Rizzo, JHEP **10**, 069 (2018) doi:10.1007/JHEP10(2018)069 [arXiv:1805.08150 [hep-ph]].
- [13] P. A. R. Ade *et al.* [Planck Collaboration], Astron. Astrophys. **594**, A13 (2016) [arXiv:1502.01589 [astro-ph.CO]].
- [14] H. Liu, T. R. Slatyer and J. Zavala, Phys. Rev. D **94**, no. 6, 063507 (2016) [arXiv:1604.02457 [astro-ph.CO]]. See also, M. Dutra, M. Lindner, S. Profumo, F. S. Queiroz, W. Rodejohann and C. Siqueira, arXiv:1801.05447 [hep-ph].
- [15] See, for example, Y. Zhang, Phys. Dark Univ. **15**, 82 (2017) [arXiv:1611.03492 [hep-ph]]; A. Ahmed, M. Duch, B. Grzadkowski and M. Iglicki, arXiv:1710.01853 [hep-ph].
- [16] G. R. Dvali, G. Gabadadze and M. A. Shifman, Phys. Lett. B **497**, 271 (2001) [hep-th/0010071]; M. Carena, E. Ponton, T. M. P. Tait and C. E. M. Wagner, Phys. Rev. D **67**, 096006 (2003) [hep-ph/0212307]; M. Carena, T. M. P. Tait and C. E. M. Wagner, Acta Phys. Polon. B **33**, 2355 (2002) [hep-ph/0207056]; F. del Aguila, M. Perez-Victoria and J. Santiago, Acta Phys. Polon. B **34**, 5511 (2003) [hep-ph/0310353] and JHEP **0302**, 051 (2003) [hep-th/0302023]; H. Davoudiasl, J. L. Hewett and T. G. Rizzo, Phys. Rev. D **68**, 045002 (2003) [hep-ph/0212279] and JHEP **0308**, 034 (2003) [hep-ph/0305086].
- [17] See, for example, B. Patt and F. Wilczek, [arXiv:hep-ph/0605188 [hep-ph]]; S. Gopalakrishna, S. Jung and J. D. Wells, Phys. Rev. D **78**, 055002 (2008) doi:10.1103/PhysRevD.78.055002 [arXiv:0801.3456 [hep-ph]]; J. D. Clarke, R. Foot and R. R. Volkas, JHEP **02**, 123 (2014) doi:10.1007/JHEP02(2014)123 [arXiv:1310.8042 [hep-ph]]; J. Liu, X. P. Wang and F. Yu, JHEP **06**, 077 (2017) doi:10.1007/JHEP06(2017)077 [arXiv:1704.00730 [hep-ph]]; L. Darm, S. Rao and L. Roszkowski, JHEP **03**, 084 (2018) doi:10.1007/JHEP03(2018)084 [arXiv:1710.08430 [hep-ph]]; J. L. Feng, I. Galon, F. Kling and S. Trojanowski, Phys. Rev. D **97**, no.5, 055034 (2018) doi:10.1103/PhysRevD.97.055034 [arXiv:1710.09387 [hep-ph]].
- [18] For a recent update, see D. Sperka (ATLAS Collaboration) and A.C. Marini (CMS Collaboration), talks given at the *53rd Rencontres de Moriond Electroweak Interactions and Unified Theories*, La Thuile, Italy, 10-17 March 2018.
- [19] C. Csaki, C. Grojean, H. Murayama, L. Pilo and J. Terning, Phys. Rev. D **69**, 055006 (2004) doi:10.1103/PhysRevD.69.055006 [arXiv:hep-ph/0305237 [hep-ph]]; C. Csaki, C. Grojean, L. Pilo and J. Terning, Phys. Rev. Lett. **92**, 101802 (2004) doi:10.1103/PhysRevLett.92.101802 [arXiv:hep-ph/0308038 [hep-ph]].
- [20] See the sixth paper in [10]
- [21] For earlier related work employing a modified warped RS setup, see K. L. McDonald and D. E. Morrissey, JHEP **1005**, 056 (2010) [arXiv:1002.3361 [hep-ph]] and JHEP **1102**, 087 (2011) [arXiv:1010.5999 [hep-ph]]; K. R. Dienes and B. Thomas, Phys. Rev. D **85**, 083523 (2012) [arXiv:1106.4546 [hep-ph]] and Phys. Rev. D **85**, 083524 (2012) [arXiv:1107.0721 [hep-ph]] and subsequent works.
- [22] See, for example, H. Liu and T. R. Slatyer, arXiv:1803.09739 [astro-ph.CO]; S. Clark, B. Dutta, Y. Gao, Y. Z. Ma and L. E. Strigari, arXiv:1803.09390 [astro-ph.HE]; A. Mitridate and A. Podo, arXiv:1803.11169 [hep-ph].

- [23] G. Steigman, Phys. Rev. D **91**, no. 8, 083538 (2015) [arXiv:1502.01884 [astro-ph.CO]].
- [24] See, for example, A. Muck, A. Pilaftsis and R. Ruckl, Phys. Rev. D **65**, 085037 (2002) [hep-ph/0110391]; T. Flacke, A. Menon and D. J. Phalen, Phys. Rev. D **79**, 056009 (2009) [arXiv:0811.1598 [hep-ph]].
- [25] S. Casagrande, F. Goertz, U. Haisch, M. Neubert and T. Pfoh, JHEP **0810**, 094 (2008) [arXiv:0807.4937 [hep-ph]].
- [26] J. Hirn and V. Sanz, Phys. Rev. D **76**, 044022 (2007) [hep-ph/0702005 [HEP-PH]].
- [27] P. Gondolo and G. Gelmini, Nucl. Phys. B **360**, 145-179 (1991)
- [28] J. L. Feng and J. Smolinsky, Phys. Rev. D **96**, no. 9, 095022 (2017) [arXiv:1707.03835 [hep-ph]] . See also, B. Li and Y. F. Zhou, Commun. Theor. Phys. **64**, no. 1, 119 (2015) [arXiv:1503.08281 [hep-ph]].
- [29] T.T. Yu (SENSEI Collaboration), talk given at the 2018 UCLA Dark Matter meeting, UCLA, 21-23 Feb. 2018.
- [30] R. Essig, T. Volansky and T. T. Yu, Phys. Rev. D **96**, no. 4, 043017 (2017) [arXiv:1703.00910 [hep-ph]].
- [31] R. Essig, M. Fernandez-Serra, J. Mardon, A. Soto, T. Volansky and T. T. Yu, JHEP **1605**, 046 (2016) [arXiv:1509.01598 [hep-ph]].
- [32] K. Saikawa and S. Shirai, [arXiv:2005.03544 [hep-ph]].
- [33] C. Csaki, [arXiv:hep-ph/0404096 [hep-ph]].